Title: PRRT2 as an auxiliary regulator of Nav channel slow inactivation

Authors: Bin Lu[1,3,9*], Qi-Wu Xu[1,9], Jing Zhang[1,9], Xue-Mei Wu[1,2,9], Jun-Yan He[1,3,9], Jing-Qiu Peng[1,2], Guang Yang[1,3,7], Ke-Xian Li[4], Ling Zhuang[1,3,8], Yu-Xian Zhang[1], Zhi-Ying Wu[6] and Zhi-Qi Xiong[1,2,3,5,10*]

Affiliations:

[1]Center for Excellence in Brain Science and Intelligence Technology (Institute of Neuroscience), Chinese Academy of Sciences, Shanghai 200031, China

[2]School of Life Science and Technology, ShanghaiTech University, Shanghai 201210, China

[3]University of Chinese Academy of Sciences, Beijing 100049, China

[4]Department of Neurology, Zhongshan Hospital, Fudan University, Shanghai 200032, China

[5]Shanghai Center for Brain Science and Brain-Inspired Intelligence Technology, Shanghai 201210, China

[6]Department of Medical Genetics and Center for Rare Diseases, Second Affiliated Hospital, Zhejiang University School of Medicine and Zhejiang Key Laboratory of Rare Diseases for Precision Medicine and Clinical Translation, Hangzhou, Zhejiang 310009, China.

[7]Present address: Interdisciplinary Research Center on Biology and Chemistry, Shanghai Institute of Organic Chemistry, Chinese Academy of Sciences, Shanghai 201210, China

[8]Present address: Hainan Academy of Medical Sciences, Hainan Medical University, Hainan 571199, China

[9]These authors contributed equally: Bin Lu, Qi-Wu Xu, Jing Zhang, Xue-Mei Wu, Jun-Yan He.

[10]Lead contact

[*]Correspondence: lubin@ion.ac.cn (B.L.), xiongzhiqi@ion.ac.cn (Z-Q.X.)

Abstract

During sustained activity, voltage-gated sodium (Nav) channels enter a slow-inactivated state to limit cellular hyperexcitability. Disruption of this regulatory process has been implicated in skeletal, cardiac and neurological disorders. While the kinetics of this process are well characterized, its endogenous modulators remain unclear. Here, we identify Proline-Rich Transmembrane Protein 2 (PRRT2) as a native regulator of Nav channel slow inactivation. We show that PRRT2 facilitates the entry of Nav channels into the slow-inactivated state and delays their recovery, a regulatory effect conserved from zebrafish to humans. PRRT2 forms

molecular complexes with Nav channels both *in vitro* and *in vivo*. In the mouse cortex, PRRT2 deficiency impairs the slow inactivation of Nav channels in neuronal axons, leading to reduced cortical resilience in response to hyperexcitable challenges. Together, these findings establish PRRT2 as a physiological modulator of Nav channel slow inactivation and reveal a mechanism that supports cortical resilience to pathological perturbations.

Introduction

Voltage-gated sodium (Nav) channels are critical for the initiation and propagation of electrical signals in excitable cells, contributing to cellular excitability in various tissues(Hodgkin & Huxley, 1952; Ulbricht, 1977). In mammals, including humans, Nav channels consist of nine α-subunit isoforms (Nav1.1-Nav1.9), which are differentially expressed and distributed across different tissues to regulate specific physiological functions(Catterall, Goldin, & Waxman, 2005). Mutations in Nav channels that lead to either loss- or gain-of-function of these channels are associated with a wide spectrum of diseases, including neurological disorders(Escayg & Goldin, 2010; Hedrich, Lauxmann, & Lerche, 2019; Meisler, Hill, & Yu, 2021), pain syndromes(Dib-Hajj, Geha, & Waxman, 2017; Waxman, 2013), muscle illnesses(Cannon, 2018; Mantegazza, Cestele, & Catterall, 2021) and cardiac diseases(Remme, 2013). Consequently, the Nav channels are considered promising therapeutic targets for treating these conditions(Noreng, Li, & Payandeh, 2021; Wisedchaisri & Gamal El-Din, 2022).

Voltage-dependent conformational changes enable Nav channels to transition between resting, open and inactivated states(Catterall, Wisedchaisri, & Zheng, 2020). Eukaryotic Nav channels undergo two major forms of inactivation (fast and slow inactivation), which are distinguished by their kinetics of onset and recovery(Goldin, 2003). Fast inactivation is triggered within milliseconds by brief depolarization and is rapidly reversed upon hyperpolarization, typically within tens of milliseconds (Armstrong & Bezanilla, 1977; Bezanilla & Armstrong, 1977). In contrast, slow inactivation develops during prolonged depolarizations and the slow inactivated channels require substantially longer periods to recover, ranging from hundreds of milliseconds to minutes(Rudy, 1978). Previous studies have shown that slow inactivation regulates Nav channel availability during sustained depolarization or high-frequency repetitive activity, thereby modulating the cellular excitability(Goldin, 2003; Silva, 2014; Vilin & Ruben, 2001). Impairment of this regulatory process due to mutations in Nav channels has been

associated with disorders such as periodic paralysis(Hayward, Sandoval, & Cannon, 1999), cardiac arrhythmias(Richmond, Featherstone, Hartmann, & Ruben, 1998; Vilin, Makita, George, & Ruben, 1999) and epilepsy(Ghovanloo et al., 2023).

Beyond the intrinsic hierarchical gating mechanisms, auxiliary regulators further modulate Nav channel inactivation dynamics(Goldin, 2003). For example, β subunits of sodium channels (SCN1B) regulate inactivation of Nav channels in the heterologous expression system, although their effects vary across different Nav isoforms and cell types(He & Soderlund, 2014; Vilin et al., 1999; Webb, Wu, & Cannon, 2009). Fibroblast growth factor homologous factors (FHFs) interact with the carboxy terminus of Nav channels(Gade, Marx, & Pitt, 2020; Goetz et al., 2009), promoting intermediated or long-term inactivation, with recovery times spanning hundreds of milliseconds(Dover, Solinas, D'Angelo, & Goldfarb, 2010; Venkatesan, Liu, & Goldfarb, 2014). Although these auxiliary proteins have been identified as regulators of fast or intermediate inactivation, native modulators that specifically target slow inactivation of Nav channels remain largely unknown.

Recent studies on proline-rich transmembrane protein 2 (PRRT2) provide new insights into this issue. The *PRRT2*, a member of the Dispanins B subfamily (DspB)(Sallman Almen, Bringeland, Fredriksson, & Schioth, 2012), has been identified as a causative gene for paroxysmal kinesigenic dyskinesia(W. J. Chen et al., 2011; Lee et al., 2012; J. L. Wang et al., 2011). *In vitro* studies have shown that PRRT2 regulates Nav channel surface expression and delays recovery of these channels from inactivated states induced by brief depolarization(Fruscione et al., 2018; Lu et al., 2021; Valente et al., 2023). However, these studies did not clearly distinguish between the effects of PRRT2 on fast versus slow inactivation, nor did they provide direct *in vivo* evidence for its role in regulating Nav channel inactivation. Our original observations that PRRT2 expression increased the accumulation of inactivated Nav channels during repetitive stimulation(Lu et al., 2021) suggest that PRRT2 may be a previously unrecognized auxiliary regulator of Nav channel slow inactivation.

In this study, we combined whole-cell voltage-clamp recordings, co-immunoprecipitation, and *in vivo* approaches to investigate the role of PRRT2 in regulating Nav channel slow inactivation, and to examine how deficits in PRRT2-mediated modulation of this process affects neuronal function in awake mice.

Results

PRRT2 regulates the slow inactivation of Nav1.2 channels

Fast and slow inactivation of Nav channels proceed through distinct gating pathways(Goldin, 2003). Although previous studies have implicated PRRT2 in the regulation of Nav channel inactivation(Fruscione et al., 2018; Lu et al., 2021), it remains unclear whether PRRT2 primarily influences fast inactivation, slow inactivation or both. To address this, we expressed mouse PRRT2 in HEK293T cells stably expressing Nav1.2 (Figure 1A) and applied classic electrophysiological paradigms to distinguish between the two inactivation processes.

Fast inactivation of Nav channels is rapidly triggered by brief depolarization and manifests as a current decay following a transient pore opening (Figure 1B and 1C), consistent with previous reports(Misra, Kahlig, & George, 2008; Thompson et al., 2023). To evaluate the kinetics of fast inactivation, we measured the time constant of current decay across a range of test potentials and found that PRRT2 expression did not significantly alter the rate at which Nav channels entered the fast-inactivated state (Figure 1C). Moreover, the majority of Nav1.2 channels recovered from fast inactivation within ~10 ms at a hyperpolarized potential of -120 mV, and PRRT2 expression had a minimal effect on this recovery (Figure 1D).

In contrast to fast inactivation, Nav channel slow inactivation develops and recovers over much longer timescales (Figure 1E), typically ranging from hundreds of milliseconds to seconds, or even to minutes(Silva, 2014). Because slow-inactivated channels do not recover during brief hyperpolarization, they can be functionally distinguished from fast-inactivated channels using a classic two-pulse protocol. In this approach, a brief hyperpolarization step (e.g., -120 mV, 10 ms) is inserted between a conditioning pulse and a test pulse to recover fast-inactivated channels. Channels that have entered the slow-inactivated state remain unavailable during the test pulse, resulting in a reduction in peak sodium current (Figure 1E)(Featherstone, Richmond, & Ruben, 1996).

To assess the development of slow inactivation, we applied depolarization pulses of variable duration, followed by a fixed 10-ms hyperpolarization before the test pulse (Figure 1F). We found that a 5-second depolarization at 0 mV was sufficient to drive most Nav1.2 channels into the slow-inactivated state (Figure 1F), consistent with previous studies(Ganguly,

120 Thompson, & George, 2021). PRRT2 significantly promoted the entry of Nav1.2 channels into
121 the slow-inactivated state during sustained depolarization (Figure 1F).
122 To examine the role of PRRT2 in channel recovery from slow inactivation, we used a protocol
123 in which a fixed 5-second depolarization at 0 mV was followed by varying durations of hy-
124 perpolarization at -120 mV to allow channel repriming (Figure 1G). PRRT2 expression mark-
125 edly slowed the recovery of Nav channels from the slow-inactivated state (Figure 1G).
126 To further investigate whether the regulation of PRRT2 in slow inactivation is voltage depend-
127 ent, we performed a steady-state slow inactivation protocol. In this assay, 10-s depolarizing
128 steps from -110 to -10 mV were applied to drive Nav channels into steady state, followed by a
129 fixed hyperpolarization and a test pulse to assess channel availability (Figure 1-figure supple-
130 ment 1A). We found that PRRT2 promotes the transition of Nav channels into the slow-inacti-
131 vated state across a broad range of membrane potentials. PRRT2 expression induced a pro-
132 nounced hyperpolarizing shift in the inactivation curve, with a $V_{0.5}$ of -76.27 mV compared to -
133 48.05 mV in controls (Figure 1-figure supplement 1B).
134 In addition to prolonged depolarization, high-frequency repetitive depolarization can also in-
135 duce Nav channel slow inactivation(Mickus, Jung, & Spruston, 1999). To determine whether
136 PRRT2 regulates slow inactivation under these conditions, we applied a pulse-train protocol
137 with an inter-pulse recovery interval of 10 ms. The use-dependent attenuation of peak sodium
138 current was quantified as the fraction of current remaining across successive depolarizations
139 (Figure 1-figure supplement 1C). Compared with the EGFP control, PRRT2 expression pro-
140 duced a greater decline in peak current during the train, consistent with enhanced slow inacti-
141 vation during repetitive depolarizations (Figure 1-figure supplement 1C). Together, these find-
142 ings indicate that PRRT2 is a potent regulator of Nav1.2 channel slow inactivation *in vitro*.
143 **Functional auxiliary factors in the regulation of Nav channel slow inactivation**
144 Several auxiliary factors of Nav channels have been identified, including the SCN1B and
145 FHF2A (also known as FGF13a), both of which are implicated in modulating Nav channel in-
146 activation(Dover et al., 2010; Isom et al., 1992). In this study, we compared the effects of
147 mouse SCN1B and FGF13a with those of PRRT2 on the development and recovery of Nav
148 channel slow inactivation (Figure 2A).

149 We found that SCN1B had negligible effects on both the entry into and recovery from the
150 slow-inactivated state of Nav1.2 compared to controls (Figures 2B and C). In contrast,
151 FGF13a markedly accelerated the onset of inactivation (Figure 2B), consistent with previous
152 reports(Dover et al., 2010; Venkatesan et al., 2014). Notably, FGF13a had minimal effect on
153 the recovery of Nav channels from the slow-inactivated state induced by a 5-second depolari-
154 zation (Figure 2C). These distinct effects of FGF13a on inactivation are consistent with the
155 idea that FGF13a does not primarily modulate classical slow inactivation, but rather promotes
156 a form of rapid-onset and long-term inactivation(Dover et al., 2010; Venkatesan et al., 2014).
157 By comparison, PRRT2 uniquely regulated slow inactivation by both facilitating entry into and
158 delaying recovery from the slow-inactivated state of Nav channels (Figures 2B and C).
159 The rodent *Prrt2* gene encodes a 346-amino-acid protein containing a proline-rich domain in
160 the N-terminus, a re-entrant loop, and a transmembrane domain in the C-terminus (Figure
161 2D). To identify the functional domain(s) responsible for regulating slow inactivation, we gen-
162 erated a series of protein-truncating variants (Figure 2D).
163 We first examined PRRT2(222–346), which lacks the N-terminal proline-rich domain (Figure
164 2D). This variant retained activity similar to the full-length PRRT2, enhancing slow inactivation
165 development and delaying recovery (Figures 2E and F). A shorter construct, PRRT2(256–
166 346), which retains the intact C-terminus, also preserved regulatory function in modulating
167 slow inactivation compared to the EGFP control (Figures 2E and F). To further test whether
168 the C-terminal region is necessary for the effect of PRRT2 on Nav channel slow inactivation,
169 we examined PRRT2(1–266), a truncated variant lacking the membrane-associated C-termi-
170 nal domains (Figure 2D). Unlike variants containing the C-terminal region, PRRT2(1–266)
171 showed no detectable effect on either the development or recovery of Nav channel slow inac-
172 tivation compared to the control (Figures 2E and F). Notably, this lack of effect was not at-
173 tributable to absent expression of the truncated construct (Figure 2-figure supplement 1A and
174 B). Together, these results indicate that the C-terminal region of PRRT2, including the re-en-
175 trant loop and transmembrane domain, is both necessary and sufficient to mediate its regula-
176 tory effect on slow inactivation of Nav1.2 channels *in vitro*.
177 **Evolutionarily conserved effects of PRRT2 on Nav channel slow inactivation**

178 The *PRRT2* and *PRRT2*-like genes emerged in vertebrates and have been conserved
179 throughout evolution(Sallman Almen et al., 2012). The alignment of amino acid sequences
180 from zebrafish, mouse, and human PRRT2 revealed 77.46% identity between human and
181 mouse PRRT2, and 43.60% identity between zebrafish and mouse PRRT2 (Figures 3A and
182 B). Notably, the majority of conserved residues are located within the C-terminal region of the
183 PRRT2 proteins (Figure 3A). Given the essential role of the C-terminus of mouse PRRT2 in
184 regulating Nav channel slow inactivation, we examined whether PRRT2 proteins from differ-
185 ent species exhibit similar effects.
186 By comparing the effects of zebrafish, mouse, and human PRRT2 on Nav channel slow inac-
187 tivation, we found that all three PRRT2 orthologs similarly promoted the entry of Nav1.2 chan-
188 nels into the slow-inactivated state (Figure 3C). Notably, in recovery assays, zebrafish PRRT2
189 was more effective at delaying the recovery process compared to its mammalian counterparts
190 (Figure 3D). To identify the domain responsible for this enhanced effect, we generated a chi-
191 meric PRRT2 construct by fusing the C-terminal region of zebrafish PRRT2 to the N-terminal
192 region of human PRRT2 (Figure 3E). The chimeric PRRT2 exhibited comparable effects on
193 the rate of slow inactivation development to those observed with both human and zebrafish
194 PRRT2 (Figure 3F). Notably, the chimeric variant displayed enhanced modulation of recovery,
195 resembling zebrafish PRRT2 and significantly differing from human PRRT2 (Figure 3G).
196 These findings indicate that the C-terminal region of zebrafish PRRT2 confers its greater abil-
197 ity to modulate recovery of Nav1.2 from the slow-inactivated state.
198 We next extended our analysis to other DspB family members, including *Trafficking regulator*
199 *of GLUT4-1* (*trarg1*) and *Transmembrane protein 233* (*tmem233*), both of which encode pro-
200 teins with C-terminal regions similar to that of PRRT2 (Figure 3-figure supplement 1A and B).
201 Given the critical role of the PRRT2 C-terminus in modulating slow inactivation, we hypothe-
202 sized that TRARG1 and TMEM233 might exert similar regulatory effects. Under heterologous
203 expression conditions, both TRARG1 and TMEM233 facilitated the entry of Nav1.2 channels
204 into the slow-inactivated state and delayed their recovery (Figure 3-figure supplement 1C and
205 D). These effects were comparable to those observed with mouse PRRT2, although
206 TMEM233 exhibited slightly weaker modulation than PRRT2 and TRARG1 (Figure 3-figure

207 supplement 1C and D). Together, these results suggest that the role of PRRT2 in regulating
208 Nav channel slow inactivation is evolutionarily conserved.

209 **PRRT2 promotes slow inactivation across multiple human Nav channel isoforms**

210 In humans, the nine Nav channel isoforms (Nav1.1-1.9) share high sequence homology and
211 similar structural features(Goldin, 2001). To determine whether PRRT2 modulates slow inacti-
212 vation across different Nav channel isoforms, we selected Nav1.1, Nav1.4, Nav1.5, and
213 Nav1.6, which are expressed in distinct tissues and cell types, and assessed the effects of
214 human PRRT2 on their slow inactivation properties (Figures 4A-J).
215 Nav1.1, Nav1.4, and Nav1.6 displayed similar kinetics in the development and recovery of
216 slow inactivation (Figures 4B, C, E, G, H, and J). In contrast, Nav1.5 showed greater re-
217 sistance to entering the slow-inactivated state (Figures 4D and I), consistent with previous
218 findings(Richmond et al., 1998). Despite these isoform-specific differences, the heterologous
219 expression of PRRT2 consistently promoted entry of Nav channels into the slow-inactivated
220 state (Figures 4A-E) and delayed recovery from it (Figures 4F-J) across all four Nav isoforms
221 tested. These results suggest that PRRT2 modulates slow inactivation through a common
222 mechanism shared by multiple Nav channel isoforms, despite differences in their intrinsic
223 slow-inactivation properties.

224 **Association between PRRT2 and Nav channels *in vitro***

225 PRRT2 may regulate slow inactivation through association with Nav channels. To examine
226 the potential physical association between human PRRT2 and Nav1.2, we co-expressed
227 PRRT2-HA and Flag-Nav1.2 in HEK293T cells and performed co-immunoprecipitation (Co-IP)
228 assays (Figures 5A and B). As controls, cells were transfected with one of the two interacting
229 proteins (either PRRT2-HA or Flag-Nav1.2) together with the empty vectors carrying the cor-
230 responding tag of the other protein (Figures 5A and B). Immunoprecipitation using an anti-
231 Flag antibody to capture Flag-Nav1.2 successfully co-precipitated PRRT2 in the co-transfec-
232 tion group, but not in the control groups where either protein was expressed (Figure 5A). Con-
233 versely, immunoprecipitation with anti-HA antibody showed that Nav1.2 was specifically co-
234 precipitated with PRRT2-HA in the co-transfection group but not in controls (Figure 5B).
235 These results confirm that PRRT2 and Nav1.2 formed a protein complex *in vitro*.

236 To identify the Nav1.2-associating region within human PRRT2, we generated truncated con-
237 structs encoding either the N-terminus (residues 1–268) or C-terminus (residues 250–340) of
238 PRRT2. Using the same Co-IP approach, we found that PRRT2(1–268), which contains the
239 intracellular proline-rich domain, failed to associate with Nav1.2 (Figures 5C-E). In contrast,
240 the PRRT2(250–340), which includes the re-entrant loop and transmembrane domain, was
241 able to interact with Nav1.2 (Figures 5F-H). These results indicate that the C-terminal region
242 of PRRT2 is necessary and sufficient, in this assay, for association with Nav1.2 channels.
243 Given that PRRT2 modulates slow inactivation across multiple Nav isoforms, we hypothe-
244 sized that it might also associate with other Nav isoforms, such as Nav1.1. To test this, we co-
245 expressed PRRT2-HA and Flag-Nav1.1 in HEK293T cells and performed Co-IP assays. Un-
246 der these conditions, PRRT2 was found to associate with Nav1.1 (Figures 5I and J), similar to
247 the association observed with Nav1.2 (Figures 5A and B).
248 These findings contrast with previous reports, which suggested that PRRT2 preferentially in-
249 teracted with Nav1.2 over Nav1.1 *in vitro*(Franchi et al., 2023; Fruscione et al., 2018; Valente
250 et al., 2023). This discrepancy may stem from differences in the experimental conditions used
251 to assess protein-protein interactions. For example, in our study, Nav1.1 and PRRT2 were co-
252 expressed in HEK293T cells, and cells were solubilized using the detergent n-Dodecyl β-D-
253 maltoside (DDM). Variations in experimental conditions could influence the stability of the
254 PRRT2-Nav channel complex and the efficiency of the Co-IP assay.
255 Collectively, our findings suggest that PRRT2 associates with Nav channels through its mem-
256 brane-associated C-terminal domains, forming molecular complexes *in vitro*.
257 **PRRT2 forms a molecular complex with Nav1.2 in the mouse brain**
258 To extend our findings from the heterologous expression system to an *in vivo* context, we first
259 investigated whether PRRT2 forms a protein complex with Nav channels in brain tissue. Due
260 to the limited efficacy of available antibodies for immunoprecipitating native PRRT2 or Nav1.2
261 from brain lysates, we employed a tag-based capture strategy, which relies on the appropriate
262 insertion of a commonly used epitope tag into the target protein.
263 We generated *Prrt2-V5* knock-in mice via CRISPR/Cas9 technology(Yang, Wang, &
264 Jaenisch, 2014), in which a V5 epitope tag was inserted at the C-terminus of PRRT2 (Figures
265 6A and B). Notably, compared with wild-type mice, PRRT2 protein levels in tissue lysates

266 were markedly reduced in *Prrt2-V5* knock-in mice (Figure 6C-D). These mice displayed sus-
267 ceptibility to dystonia attacks, resembling the phenotype previously observed in *Prrt2*-mutant
268 mice(Wu et al., 2025), but with lower penetrance (Figure 6-figure supplement 1A-C).
269 Despite the reduced PRRT2 expression, Nav1.2 expression remained unchanged (Figure
270 6E), and co-immunoprecipitation assays remained effective in the *Prrt2-V5* knock-in mice. Us-
271 ing anti-V5 nanobody-conjugated magnetic beads, PRRT2 was effectively immunoprecipi-
272 tated from membrane lysates of brain tissue (Figure 6C). A notable amount of Nav1.2 was co-
273 immunoprecipitated in the *Prrt2-V5* knock-in group, whereas only trace levels were detected
274 in wild-type controls (Figures 6C and F). In contrast, ATP1B2, another membrane protein,
275 was not co-immunoprecipitated in the *Prrt2-V5* knock-in group (Figures 6C and F), supporting
276 the specificity of the association between PRRT2 and Nav1.2. Together, although the *V5*
277 knock-in allele is hypomorphic, these results provide *in vivo* evidence that PRRT2 forms a
278 molecular complex with Nav1.2 channels in the mouse brain.

279 **PRRT2 deficiency impairs the regulation of Nav channel slow inactivation in cortical**
280 **neuronal axons**

281 Given the dense distribution of both PRRT2 and Nav channels in the cerebral and cerebellar
282 cortices(Yamano, Miyazaki, & Nukina, 2022), we next investigated whether PRRT2 regulates
283 Nav channel slow inactivation in cortical neurons. Cortical slices were prepared from wild-type
284 and *Prrt2*-mutant mice, the latter lacking PRRT2 expression(Tan et al., 2018). Unlike the rela-
285 tively simple morphology of HEK293T cells, pyramidal neurons have complex arborizations,
286 which present space-clamp limitations during whole-cell voltage-clamp recordings(Bar-Ye-
287 huda & Korngreen, 2008). To mitigate these issues, we followed established protocols to iso-
288 late axonal blebs from cortical pyramidal neurons(Hu & Shu, 2012). These spherical, mem-
289 brane-bound blebs form at the cutting surface of cortical slices and are readily visualized (Fig-
290 ure 7A). Sodium currents recorded from axon blebs were voltage-dependent and sensitive to
291 tetrodotoxin (TTX) (Figure 7A), confirming that they were primarily mediated by Nav chan-
292 nels(Hu & Shu, 2012).
293 PRRT2 deficiency did not affect Nav1.2 protein expression in forebrain tissues (Figure 7-fig-
294 ure supplement 1A and B), nor did it alter the sodium current density in cortical axonal blebs
295 when measured with a brief depolarization to 0 mV preceded by a 200-ms hyperpolarizing

296 prepulse to -110 mV, a protocol designed to relieve inactivation before current elicitation (Fig-
297 ure 7B). Because prolonged voltage-clamp recordings from isolated axonal blebs are techni-
298 cally challenging, we adopted a simplified protocol to assess Nav channel slow inactivation,
299 using a holding potential of -70 mV to approximate the resting membrane potential of cortical
300 neurons. In this protocol, a single 5-s depolarization to 0 mV was applied, and the fraction of
301 available Nav channels was determined after a 10-ms hyperpolarization (Figure 7C).
302 Approximately 20% of available sodium current remained in wild-type blebs, compared to
303 ~40% in *Prrt2*-mutant blebs (Figures 7C and D), indicating that during sustained depolariza-
304 tion, fewer Nav channels in the *Prrt2*-mutant group entered the slow-inactivated state. Nota-
305 bly, because the proportion of channels entering slow inactivation differed substantially be-
306 tween wild-type and *Prrt2*-mutant groups, direct comparison of recovery kinetics was not fea-
307 sible and was therefore not performed. Nevertheless, these findings provide direct evidence
308 that endogenous PRRT2 is required for effective regulation of Nav channel slow inactivation
309 in cortical neurons.

310 **PRRT2 deficiency compromises cortical resilience in awake mice**

311 Excitatory neurons exhibit intrinsic adaptation, whereby their responses progressively decline
312 during sustained or repetitive activation(Fleidervish, Friedman, & Gutnick, 1996; Kim, Owen,
313 Holmes, & Grover, 2012). We therefore hypothesized that PRRT2 may contribute to this pro-
314 cess by promoting Nav channel slow inactivation.
315 To test this idea, we applied a repetitive stimulation protocol in the corpus callosum, a white-
316 matter region of the brain enriched in both PRRT2 and Nav channels. Compound action po-
317 tentials, recorded with a glass electrode positioned 150 μm from the stimulation site, were
318 used as a functional readout related to Nav channel availability during repetitive activity (Fig-
319 ure 7-figure supplement 2A). Compared with wild-type mice, *Prrt2*-mutant mice exhibited a
320 smaller decline in compound action potential amplitude during high-frequency stimulation (20
321 Hz), but not during low-frequency stimulation (1 Hz), indicating reduced adaptation (Figure 7-
322 figure supplement 2B and C). This pattern is consistent with impaired slow inactivation during
323 repetitive activity.
324 Neuronal adaptation is important for limiting excitability during episodes of aberrant network
325 hyperactivity (Fleidervish et al., 1996; Zang, Marder, & Marom, 2023). To further determine

326 whether PRRT2-dependent impairment of neuronal adaptation contributes to hyperexcitability
327 *in vivo*, we next assessed cortical resilience in awake mice, a measure of the resistance of
328 the cerebral cortex to pathological perturbations. We used a stimulation-response paradigm in
329 which stimulating electrodes were implanted into the left cerebral cortex, targeting both the
330 sensory and visual cortices, while EEG recording electrodes were placed in the contralateral
331 hemisphere, which receives projections from the stimulated region (Figure 7E). Pulsed electri-
332 cal stimulation (1-ms pulse width at 60 Hz for 2 s) was delivered to the cortex of mice once
333 daily with stepwise increases in current intensity, and the minimal current required to evoke
334 after-discharges (ADs) in the contralateral cortex was determined in each animal (Figure 7F).
335 The threshold current required to induce after-discharges was used as a functional indicator
336 of cortical resilience to aberrant excitatory inputs(Blume, Jones, & Pathak, 2004).
337 *Prrt2*-mutant mice exhibited significantly lower stimulation thresholds for evoking after-dis-
338 charges compared to wild-type controls (Figures 7G and H). Specifically, stimulation at an av-
339 erage intensity of 85 μA reliably induced after-discharges in *Prrt2*-mutant mice, whereas a
340 significantly higher intensity (190 μA) was required to elicit similar responses in wild-type mice
341 (Figures 7H and I), indicating that PRRT2 contributes importantly to maintaining cortical resili-
342 ence in response to excitatory perturbations.

343 **Discussion**

344 In this study, we identified PRRT2 as a physiological auxiliary factor of Nav channel slow inac-
345 tivation. We demonstrate that PRRT2 exerts a dual action by both facilitating the transition of
346 Nav channels into a slow-inactivated state and delaying their recovery. Importantly, this regu-
347 latory action is evolutionarily conserved, and requires the integrity of the PRRT2 C-terminal
348 region. Using both *Prrt2-V5* knock-in and *Prrt2*-mutant mouse models, we provide compelling
349 *in vivo* evidence that PRRT2 forms a molecular complex with Nav channels and modulates
350 their slow inactivation, thereby contributing to neuronal adaptation and cortical resilience to
351 perturbations.

352 In eukaryotic Nav channels, ion permeability is regulated through at least four distinct and co-
353 ordinated gating mechanisms: voltage-gated activation and deactivation, fast inactivation, and
354 slow inactivation(Catterall, 2023). Slow inactivation, an evolutionarily conserved intrinsic prop-
355 erty of Nav channels, is mediated by conformational rearrangements and has distinct

356 molecular determinants from those governing fast inactivation(Payandeh, 2018; Silva, 2014;
357 Vilin & Ruben, 2001).
358 The role of PRRT2 in the regulation of Nav channel slow inactivation appears to be unique
359 compared to known regulators such as SCN1B and FHFs. The modulatory effects of the
360 SCN1B on Nav channel inactivation were initially observed in *Xenopus* oocytes(Wallner,
361 Weigl, Meera, & Lotan, 1993), where it was found to influence sodium currents. Subsequent
362 studies proposed that the SCN1B impedes slow inactivation, a hypothesis later confirmed in
363 mammalian cells co-expressing Nav1.4 and SCN1B(Webb et al., 2009). However, its regula-
364 tory effects on slow inactivation varied across Nav isoforms(He & Soderlund, 2014; Makita,
365 Bennett, & George, 1996; Vilin et al., 1999; Xu et al., 2007). In this study, we observed little
366 effect of SCN1B on the onset and recovery of slow inactivation in Nav1.2, consistent with pre-
367 vious findings(Xu et al., 2007). In contrast to SCN1B, PRRT2 exerts a more consistent effect
368 across Nav isoforms, enhancing slow inactivation regardless of the specific Nav subtype.
369 FHF proteins (FHF1-4, also known as FGF11-14) constitute a subfamily of FGFs that lack a
370 secretion signal and function distinctly from traditional FGFs(Olsen et al., 2003). Previous
371 studies demonstrated that FHFs mediate a rapid-onset, long-term inactivation, which differs
372 mechanically from traditional slow inactivation(Dover et al., 2010). Unlike the FHF2A-medi-
373 ated long-term inactivation, which can be triggered by a brief 2-ms depolarization, PRRT2 re-
374 quires a longer depolarization to produce a detectable effect on the onset of slow inactivation
375 of Nav channels. Additionally, PRRT2 significantly delays recovery of Nav channels from the
376 slow-inactivated state induced by 5-second depolarization, whereas FHF2A has little effect on
377 this process. These findings suggest that PRRT2 and FHF2A modulate Nav channel inactiva-
378 tion through different mechanisms.
379 Previous studies in heterologous overexpression systems have shown that PRRT2 can influ-
380 ence Nav channel trafficking and surface expression(Fruscione et al., 2018; Valente et al.,
381 2023), raising the possibility that the observed effects on slow inactivation are secondary to
382 altered channel abundance or localization. However, slow inactivation develops on a time-
383 scale of tens of milliseconds to seconds, whereas detectable changes in Nav channel traffick-
384 ing and surface abundance generally occur over much longer intervals (minutes to hours)
385 (Freal et al., 2023; Higerd-Rusli et al., 2023). These distinct temporal profiles argue against

386 trafficking as the primary basis for the effects of PRRT2 on Nav channel slow inactivation de-
387 scribed here, although direct quantification of dynamic changes in Nav channel surface ex-
388 pression will be required to fully exclude such a contribution(Liu, Wang, Pitt, & Liu, 2022;
389 Tyagi, Higerd-Rusli, Akin, Waxman, & Dib-Hajj, 2025).
390 Our truncation analysis showed that the C-terminal region of PRRT2, which contains the re-
391 entrant loop and transmembrane domain, is sufficient to reproduce the enhancement of slow
392 inactivation. This finding suggests that PRRT2 modulates slow inactivation through a mem-
393 brane-embedded or membrane-proximal mechanism, rather than through its intracellular pro-
394 line-rich N-terminus. Current models of Nav channel slow inactivation propose that entry into
395 the slow-inactivated state involves coupled conformational changes in both the voltage-sens-
396 ing domains and the pore region(Catterall, Gamal El-Din, & Wisedchaisri, 2024; Silva, 2014),
397 including contributions from the external pore mouth(Balser et al., 1996; Xiong et al., 2006),
398 the selectivity filter(Chatterjee et al., 2018; Todt, Dudley, Kyle, French, & Fozzard, 1999), the
399 S6 segments(Chancey, Shockett, & O'Reilly, 2007; Y. Chen, Yu, Surmeier, Scheuer, &
400 Catterall, 2006; S. Y. Wang & Wang, 1997), and regions encompassing S4, S4-S5 linker, and
401 S5 (Bendahhou, Cummins, Kula, Fu, & Ptacek, 2002; Cummins & Sigworth, 1996; Hayward
402 et al., 1999; Mitrovic, George, & Horn, 2000; D. W. Wang, Makita, Kitabatake, Balser, &
403 George, 2000). Within this framework, the membrane-associated C-terminal region of PRRT2
404 may enhance slow inactivation by stabilizing one or both of these conformational rearrange-
405 ments, although the precise structural basis of this effect remains to be determined.
406 In mammals, Nav channel isoforms (Nav1.1–1.9) are distributed across the nervous system,
407 skeletal muscle, heart and secretory glands(Cusdin, Clare, & Jackson, 2008). Although we
408 have shown that PRRT2 exerts a consistent effect on slow inactivation across various Nav
409 channel isoforms *in vitro*, the regulation of Nav channel slow inactivation is likely to be more
410 complex under physiological conditions. PRRT2 is predominantly expressed in the nervous
411 system(W. J. Chen et al., 2011), with enrichment in excitatory neurons(Tan et al., 2018), mak-
412 ing it unlikely to directly modulate Nav1.4 and Nav1.5 channels, which are primarily ex-
413 pressed in skeletal muscle and cardiac tissue, respectively(Cusdin et al., 2008). A similar ra-
414 tionale applies to Nav1.1, which is largely confined to inhibitory interneurons(Yu et al., 2006),
415 where PRRT2 expression is minimal or absent. These observations suggest that the

416 functional consequence of PRRT2 depend on the Nav isoform composition and cellular con-
417 text of each tissue.
418 The partial mismatch between PRRT2 and Nav channel expression *in vivo* raises an im-
419 portant question about how Nav channel slow inactivation is regulated in cells that do not ex-
420 press PRRT2. One possibility is the expression of alternative regulators, such as TRARG1 or
421 TMEM233, both of which belong to the DspB family and are expressed in tissues distinct from
422 PRRT2(Ehrlich, Lacey, & Ehrlich, 2020; Oort, Warden, Baumann, Knotts, & Adams, 2007;
423 Santana-Varela et al., 2021; Shibata et al., 2007). These proteins may serve analogous func-
424 tions in modulating Nav channel slow inactivation. Another possibility is that certain PRRT2-
425 negative cells have a reduced requirement for Nav channel slow inactivation modulation due
426 to their intrinsic rhythmic firing properties. For instance, in the cerebellar cortex, the PRRT2 is
427 absent in Purkinje cells, which exhibit repetitive firing(Lu et al., 2021). In such rhythmic firing
428 cells, strong enhancement of Nav channel slow inactivation may be undesirable, as excessive
429 accumulation of inactivated Nav channels could disrupt their regular firing patterns. Thus, the
430 broad isoform activity of the PRRT2 should be considered in any future attempt to manipulate
431 PRRT2 function therapeutically.
432 Given the critical role of PRRT2 in regulating Nav channel slow inactivation, its deficiency
433 would be expected to alter neuronal excitability and neuronal responses to prolonged or re-
434 petitive activity, thereby contributing to central nervous system dysfunction. Evidence from
435 cultured neurons, animal models, and human genetics is broadly consistent with this view.
436 Studies using human induced pluripotent stem cells (iPSC)-derived excitatory neurons have
437 shown that homozygous *PRRT2* mutation increases sodium currents and neuronal excitabil-
438 ity(Fruscione et al., 2018). In mouse models, loss-of-function mutation or knockout of PRRT2
439 in cerebellar granule cells increases intrinsic excitability and facilitates spreading depolariza-
440 tion in the cerebellar cortex(Binda, Valente, Marte, Baldelli, & Benfenati, 2021; Lu et al.,
441 2021), whereas in the forebrain, PRRT2 deficiency impairs Nav channel slow inactivation in
442 cortical neurons and reduces resistance to pathological perturbation in awake mice. In addi-
443 tion, *PRRT2* mutations in humans are associated with infantile convulsions(Lee et al., 2012),
444 paroxysmal dyskinesia(W. J. Chen et al., 2011; J. L. Wang et al., 2011), and hemiplegic mi-
445 graine(Riant et al., 2022), all disorders linked to abnormal neuronal network excitability.

446 Although the present study supports a functional link between PRRT2-dependent regulation
447 of Nav channel slow inactivation and cortical resilience, PRRT2 may influence cortical excita-
448 bility and stability through additional Nav-dependent mechanisms, including reduced current
449 density and shifts in the voltage dependence of channel inactivation(Fruscione et al., 2018; Lu
450 et al., 2021; Valente et al., 2023). Notably, because PRRT2 facilitates Nav channel entry into
451 slow-inactivated states both from closed states and from open states during prolonged depo-
452 larization, some of these previously reported effects may partly reflect enhanced slow inacti-
453 vation and the resulting reduction in Nav channel availability. In addition to these Nav-depend-
454 ent mechanisms, previous studies have shown that PRRT2 also regulates synaptic vesicle
455 cycling(Coleman et al., 2018; Tan et al., 2018; Valente et al., 2016) and presynaptic surface
456 expression of Cav2.1 channels(Ferrante et al., 2021). These effects are also expected to in-
457 fluence neurotransmitter release and, consequently, neuronal and network excitability, and
458 may therefore contribute to cortical resilience.
459 Together, the identification of PRRT2 as an auxiliary factor regulating Nav channel slow inacti-
460 vation provides new insight into the fine-tuning of Nav channel function and offers a mecha-
461 nistic framework for understanding how PRRT2 deficiency may contribute to episodic neuro-
462 logical disorders associated with excitability dysregulation.

463 **Limitations of the study**

464 While our study identifies the functional domain of PRRT2 and provides biological evidence
465 that PRRT2 associates with Nav1.2, the precise binding site on the Nav channel that medi-
466 ates PRRT2-dependent regulation of slow inactivation remains undefined. Direct structural
467 and biochemical mapping of the PRRT2-Nav interface, including targeted mutagenesis,
468 crosslinking, and structural determination, will be necessary to elucidate the molecular basis
469 of this interaction and its effect on channel gating. Cryo-electron microscopy (cryo-EM) repre-
470 sents a promising approach for resolving the structural details of the Nav-PRRT2 complex,
471 particularly in light of recent advancements in determining high-resolution structures of vari-
472 ous Nav channel isoforms and their complexes with auxiliary factors(Jiang et al., 2020; Pan et
473 al., 2019; Pan et al., 2021).

474 **Materials and Methods**

475 **Molecular cloning**

476 Mammalian expression constructs were generated using the pCAGIG backbone (Addgene,
477 11159), which contains an internal ribosome entry site (IRES) followed by EGFP(Matsuda &
478 Cepko, 2004). Coding sequences for full-length or truncated proteins of interest (POIs) were
479 inserted in the pCAGIG vector using a seamless cloning method (Beyotime, D7010). The
480 POIs included human PRRT2 (hPRRT2), hPRRT2(1–268), hPRRT2(250–340), mouse
481 PRRT2 (mPRRT2), mPRRT2(222–346), mPRRT2(256–346), mPRRT2(1–266), zebrafish
482 PRRT2 (zfPRRT2), mouse SCN1B, mouse FHF2A, mouse TRARG1 and mouse TMEM233.
483 A PRRT2 chimeric construct was generated by fusing the N-terminal fragment of human
484 PRRT2 (hPRRT2(1–222)) with the C-terminal region of zebrafish PRRT2 (zPRRT2(110–
485 226)), and cloning the resulting sequence into pCAGIG vector. Plasmids encoding human
486 PRRT2(W. J. Chen et al., 2011) were kindly provided by Dr. Zhi-Ying Wu's Laboratory
487 (Zhejiang University). Plasmids of pCAG-Flag-Nav1.2(Pan et al., 2019) and pCAG-Flag-
488 Nav1.1(Pan et al., 2021) were provided by Huai-Zong Shen's Laboratory (Westlake Univer-
489 sity). All constructs generated in this study were verified by Sanger sequencing (BioSune,
490 Boshang Biology Technology, Shanghai).

491 **Cell culture and heterologous expression**

492 HEK293T cell lines stably expressing human Nav1.2 or Nav1.6 and CHO cell lines stably ex-
493 pressing human Nav1.1, Nav1.4 or Nav1.5 were obtained from the laboratory of ICE Biosci-
494 ence Inc. Wild-type HEK293T cells (SCSP-502) used for transient transfection were obtained
495 from Cell Bank/Stem Cell Bank of Chinese Academy of Sciences. All cells were cultured in
496 Dulbecco's modified Eagle medium (DMEM; Gibco, 11995065) supplemented with 10% fetal
497 bovine serum (FBS; Gibco,10099141) and penicillin (50 U/mL)-streptomycin (50 μg/mL)
498 (Gibco,15140163), and maintained at 37 °C in a humidified incubator with 5% CO_2. The
499 HEK293T cell line used in this study is of female origin and tested negative for mycoplasma
500 contamination.

501 For heterologous protein expression in whole-cell voltage-clamp recording, 2 μg of plasmid
502 DNA was transfected into HEK293T or CHO cells using Lipofectamine 2000 (ThermoFisher,
503 11668-019) according to the manufacturer's instructions. For co-immunoprecipitation assays,
504 2–3 μg of total plasmid DNA (encoding two proteins of interest) was used for co-transfection.
505 Four hours after the transfection, the medium was replaced with fresh growth medium, and

506 cells were maintained for an additional 20 hours before subsequent experiments.

507 **Animals**

508 *Prrt2*-mutant mice, carrying a premature stop codon in exon 2 of the *Prrt2* gene(Tan et al.,
509 2018), were used in electrophysiological recording experiments.

510 *Prrt2-V5* knock-in mice, used for co-immunoprecipitation (Co-IP) experiments, were gener-
511 ated in this study via CRISPR/Cas9 technology(Yang et al., 2014). Briefly, single-guide RNA
512 (sgRNA: 5'-TCTCCCACAGTGTATAAGTG-3') targeting the location nearby the stop codon of
513 *Prrt2* gene allele, together with a single-stranded DNA donor template encoding a V5 tag
514 flanked by 53-bp homology arms (ssDNA: 5'-CTTCCCTGTC TGTCTTTCCC TCTCCTCTCC
515 CACAGTGTAT AAGGGCAAGC CCATCCCCAA CCCCCTGCTG GGCCTGGACA GCAC-
516 CTGAGG GGCTCTGCCC TGCATTCCAA GACTTTTCTT CCTGTTGG-3') and Cas9 mRNA,
517 were microinjected into zygotes from fertilized C57BL/6J mice. The injected zygotes were im-
518 planted into pseudopregnant female mice. Offspring were screened for correct insertion of the
519 V5 tag immediately upstream of the *Prrt2* stop codon by PCR, and the insertion was subse-
520 quently verified by Sanger sequencing. Positive founder (F0) mice were crossed with
521 C57BL/6J mice to establish the *Prrt2-V5* knock-in line.

522 Both *Prrt2*-mutant and *Prrt2-V5* lines were backcrossed onto the C57BL/6J background for
523 more than 10 generations. C57BL/6J mice used for breeding were obtained from the Shang-
524 hai Laboratory Animal Center (SLAC), Chinese Academy of Science.

525 Mice were housed in a 12-h light-dark cycle (light on at 7:00 a.m.) with ad libitum access to
526 food and water. All procedures involving animals were approved by the Animal Care and Use
527 Committee of the Center for Excellence in Brain Science and Intelligence Technology, Chi-
528 nese Academy of Sciences (Approval number, NA-009-2022). Both male and female mice
529 were used in experiments.

530 **Whole-cell voltage clamp recording for sodium currents in cell lines**

531 Sodium currents were recorded from HEK293T or CHO cell lines stably expressing individual
532 human Nav channel isoforms (ICE Bioscience Inc.). Cells were transfected with plasmids as
533 described in the main text. Twenty-four hours after transfection, cells were trypsinized and re-
534 plated at lower density onto poly-D-lysine-coated coverslips. EGFP-positive cells were se-
535 lected for recording 24 hours later.

536 Whole-cell voltage-clamp recordings were conducted at room temperature (23-24 °C). The
537 bath solution contained (in mM): 50 NaCl, 90 choline chloride, 3.5 KCl, 1 $MgCl_2$, 2 $CaCl_2$, 10
538 D-Glucose, 1.25 NaH_2PO_4, and 10 HEPES (pH adjusted to 7.4 with NaOH). The internal pi-
539 pette solution contained (in mM): 50 CsCl, 60 CsF, 10 NaCl, 20 EGTA, 10 HEPES (pH ad-
540 justed to 7.2 with CsOH). The osmolarity of the external and internal solutions was adjusted to
541 300 and 290 mOsmol/kg, respectively.
542 Pipette electrodes were pulled from borosilicate glass capillary (Sutter Instruments, BF150-
543 86-10) using a horizontal puller (P-97, Sutter Instruments). The pipette resistance was ap-
544 proximately 2 MΩ when filled with internal pipette solution. After whole-cell configuration was
545 achieved, cells were allowed to equilibrate for 5 minutes prior to recording. Series resistance
546 was compensated by 80% to minimize voltage errors. Currents were recorded with an ampli-
547 fier (HEKA, EPC-10), sampled at 10 kHz, and acquired using Patchmaster (HEKA, v2x92).
548 **Fast inactivation assay for Nav channels**
549 To assess the fast-inactivation kinetics of Nav channels, sodium currents were evoked by 20-
550 ms depolarizing steps to test potentials between -20 and +30 mV in 10-mV increments, from
551 a holding potential of -120 mV. The decay time constant (tau) was obtained by mono-expo-
552 nential fitting of the current trace.
553 Recovery from fast inactivation was measured using a two-pulse protocol, in which a 10-ms
554 depolarizing pulse to 0 mV (P1) was followed by a variable-duration recovery period at -120
555 mV and a second 10-ms test pulse at 0 mV (P2). Recovery was quantified as the normalized
556 peak current of P2 relative to P1.
557 **Slow inactivation assay for Nav channels**
558 To evaluate the development of slow inactivation of Nav channels, a series of conditioning
559 prepulses of increasing duration at 0 mV was applied, followed by a brief 10-ms recovery at
560 -120 mV and a 10-ms test pulse at 0 mV. Inter-sweep intervals were set at 15 s. Available
561 fractions of Nav channels were assessed by normalizing the peak currents in the test pulse to
562 that of the conditioning pulse.
563 For slow inactivation recovery, a 5-s conditioning pulse at 0 mV was followed by variable re-
564 covery durations at -120 mV, then a 10-ms test pulse at 0 mV. The inter-sweep interval was
565 15 s.

566 In experiments assessing the effect of zebrafish PRRT2 on slow inactivation recovery, a modi-
567 fied protocol was used to avoid cumulative inactivation. Within a single sweep, a 5-s depolari-
568 zation was followed by a series of 10-ms test pulses to 0 mV, each separated by progres-
569 sively longer recovery periods at -120 mV(Webb et al., 2009).
570 In this study, we chose 0 mV as the primary conditioning potential because it is widely used in
571 conventional slow inactivation protocols and induces slow inactivation more robustly than
572 more negative conditioning voltages, such as -70 mV.

573 **Steady-state slow inactivation assay for Nav channels**

574 To measure steady-state slow inactivation, 10-s conditioning pulses ranging from -110 to -10
575 mV (in 10 mV increments) were applied, followed by a 10-ms hyperpolarizing step to -120 mV
576 and subsequently a 5-ms test pulse to 0 mV. The peak test current was normalized to the
577 maximum sodium current recorded across all conditions in the protocol and reported as I/I_{max}.

578 **Slice preparation**

579 Mice (postnatal day 14-20) were anesthetized with 4% isoflurane. The brain tissues were rap-
580 idly extracted and immersed in ice-cold sucrose-based cutting solution containing (in mM): 2.5
581 KCl, 1.25 NaH_2PO_4, 26 $NaHCO_3$, 10 $MgSO_4$, 0.5 $CaCl_2$, 10 D-Glucose, 205 sucrose, 1 so-
582 dium pyruvate, 1.3 sodium L-ascorbate. Coronal cortical slices (250 μm) were prepared using
583 a vibratome (Leica, VT1200S).
584 Slices were then transferred immediately to an incubation beaker containing aerated artificial
585 cerebrospinal fluid (ACSF) composed of (in mM): 126 NaCl, 2.5 KCl, 2 $MgSO_4$, 2 $CaCl_2$, 26
586 $NaHCO_3$, 1.25 NaH_2PO_4 and 25 dextrose (pH 7.4, 315 mOsm). Slices were incubated at
587 35 °C for 30 min, then maintained in the same solution at room temperature until use. The ox-
588 ygenated ACSF was equilibrated with 95% O_2 and 5% CO_2.

589 **Electrical stimulation and field recording in the corpus callosum**

590 Coronal slices were transferred to a recording chamber. A stimulation electrode (125 μm in
591 diameter, concentric bipolar electrode, FHC, USA) was placed on the corpus callosum. The
592 Ag-AgCl recording electrode (2-3 MΩ) was located at a site 150 μm away from the stimulation
593 electrode along the corpus callosum. Stimulating pulses (0.1 ms pulse width, 100 μA) were
594 delivered at 1 Hz for 100 seconds or at 20 Hz for 5 seconds. Compound action potentials
595 were recorded as a functional readout related to Nav channel availability.

596 **Electrophysiological recording in isolated axonal blebs**

597 Slices were transferred to a recording chamber and stabilized with a platinum anchor grid dur-
598 ing recording. Resealed axonal ends ("blebs") in the cerebral cortex were visualized using an
599 upright infrared differential interference contrast (IR-DIC) microscope. Individual blebs were
600 mechanically isolated by sweeping a cutting pipette beneath it, and subsequently patched
601 with glass electrodes (resistance ~7 MΩ).

602 For sodium current recordings, pipettes were filled with a potassium gluconate-based internal
603 solution containing (in mM): 130 K-gluconate, 1 $MgCl_2$, 11 EGTA, 1 $CaCl_2$, 1 KCl, 2 Mg-ATP,
604 0.3 Na-GTP, 10 HEPES (pH adjusted to 7.2, ~290 mOsm), supplemented with 2 mM TEA-Cl.
605 The external ACSF solution was supplemented with 5 mM 4-Aminopydine (4-AP) and 200 μM
606 $CdCl_2$ to block K^+ and Ca^{2+} currents, respectively. 1 μM tetrodotoxin (TTX) was used to block
607 TTX-sensitive Nav channels.

608 Whole-cell voltage-clamp recordings were performed using a MultiClamp amplifier (Molecular
609 Devices, 700B). Currents were filtered at 4 kHz (low-pass) and digitized at 20 kHz via a Digi-
610 data interface (Molecular Devices, 1440A). Series resistance was compensated by 80% to
611 minimize voltage errors. Leak currents were subtracted by using an online P/4 procedure.
612 The holding potential was set to -70 mV, approximating the resting membrane potential of cor-
613 tical neurons. To assess sodium current density, a hyperpolarization prepulse to -110 mV
614 (200 ms) was used to remove inactivation, followed by a 20-ms depolarization to 0 mV. So-
615 dium current density (nA/pF) was calculated by normalizing peak current to bleb capacitance.
616 To evaluate Nav channel slow inactivation, a single 5-s depolarizing pulse (0 mV) was applied
617 to induce slow inactivation followed by test pulses (0 mV, 20 ms) separated by 10-ms recov-
618 ery intervals at -70 mV. The fraction of available Nav channels was calculated by normalizing
619 the peak current amplitude of each test pulse to the peak current measured at the onset of
620 the 5-s depolarization.

621 **Co-immunoprecipitation in transfected HEK293T cells**

622 In co-immunoprecipitation experiments, one protein-of-interest was tagged with an HA epitope
623 and the other with a Flag epitope. The pCAGIG vector bearing either a HA or Flag tag alone
624 was used as a control in paired constructs. HEK293T cells transfected with a pair of con-
625 structs were harvested 24 hours post-transfection for protein expression. Cells were lysed in

626 ice-cold lysis buffer (20 mM Tris-HCl, 150 mM NaCl, 0.5% n-Dodecyl β-D-maltoside (DDM,
627 Anatrace, D310), and protease inhibitor cocktail (Selleckchem, B14002)) with gentle agitation
628 at 4 °C for 2 hours. Lysates were centrifuged at 20,000 x g for 20 minutes at 4 °C to remove
629 insoluble debris. The supernatant was transferred to a fresh tube and kept on ice.
630 Protein concentration of supernatant was determined using a colorimetric bicinchoninic acid
631 (BCA) assay (Beyotime, P0012S). For each immunoprecipitation (IP), 400 μg of proteins was
632 incubated with 30 μL of anti-HA nanobody magnetic beads (AlfaLifeBio, KTSM1335) or anti-
633 Flag magnetic beads (Bimake, B26102) at 4 °C with rotation for 1 hour. Beads were then sep-
634 arated with DynaMag spin and washed three times with wash buffer (20 mM Tris-HCl, 150
635 mM NaCl, 0.05% DDM). The captured proteins were eluted with 25 μL SDS-PAGE loading
636 buffer containing 100 mM DTT, followed by heating at 45 °C for 10 min. Samples were stored
637 at -20 °C prior to western blot analysis.

638 **Co-immunoprecipitation in mouse brain tissues**

639 Brain tissues (~100 mg per sample) were freshly dissected from wild-type or *Prrt2-V5* knock-
640 in mice, and homogenized on ice using glass homogenizers in 1 mL of Tris-buffered saline
641 (TBS, 20 mM Tris-HCl, 150 mM NaCl, protease inhibitor cocktail). The homogenates were
642 centrifuged at 800 x g for 10 min at 4 °C to remove nuclei and cell debris. Supernatants were
643 subjected to centrifugation at 40,000 x g for 45 minutes at 4 °C to isolate membrane fractions.
644 The resulting membrane-enriched pellets were resuspended in TBS and solubilized in lysis
645 buffer containing 0.3% DDM for 3 hours at 4 °C. Lysates were then cleared by centrifugation
646 at 20,000 x g for 20 minutes at 4 °C. Protein concentration was measured via BCA assay. For
647 each IP, ~200 μg of proteins was incubated with 30 μL of V5-Trap magnetic beads (Chro-
648 motek, v5tma-20) at 4 °C with rotation for 1.5 hours. Beads were washed three times with
649 wash buffer (20 mM Tris-HCl, 150 mM NaCl, 0.15% DDM), and bound proteins were eluted
650 with 25 μL SDS-PAGE loading buffer containing 100 mM DTT, followed by heating at 45 °C
651 for 10 min. Eluates were kept at -20 °C until use in western blotting.

652 **Western blotting**

653 Protein samples were separated using 4-12% PAGE Gel (Nanjing ACE Biotechnology,
654 ET15412L) in MES-SDS running buffer at 140 V for 60 minutes. Proteins were transferred
655 onto polyvinylidene difluoride (PVDF) membranes at 300 mA for 2 hours at 4 °C. The PVDF

656 membranes were blocked in 5% nonfat milk in TBST (TBS with 0.1% Tween-20) for 1 hour at
657 room temperature, followed by incubation with indicated primary antibodies overnight at 4 °C
658 with gentle agitation.
659 After three washes in TBST, membranes were incubated with HRP-conjugated secondary an-
660 tibodies for 2 hours at room temperature. Following another three washes, chemiluminescent
661 substrate (TIANGEN Biotech, PA112) was applied, and signals were detected using a blot im-
662 aging system (Analytikjena, ChemStudio 815). Densitometric analysis of protein bands was
663 performed using QuantityOne software (Biorad, Quantity One 1-D analysis, v4.6.2). The pri-
664 mary antibodies we used in western blotting were as follows: Anti-human PRRT2 (Atlas anti-
665 bodies, HPA014447), Anti-Nav1.2 (Alomone Labs, ASC-002), Anti-Nav1.1 (Alomone Labs,
666 ASC-001), Anti-HA-Tag (Cell signaling technology, 3724S), Anti-GAPDH-HRP (KangChen
667 Bio-tech,KC-5G5), Anti-ATP1B2 (Abcam, ab185210), Anti-mouse PRRT2 (Wiiget Biotech,
668 Rp3246) and Anti-β Actin-HRP (Cell signaling technology, 5125S).
669 **Animal Surgery**
670 Mice were anesthetized with isoflurane (RWD life science, R510-22-10), using 4% for induc-
671 tion and 2% for maintenance. Body temperature was maintained throughout the procedure
672 with a heating pad. Meloxicam (5 mg/kg, subcutaneous) was administered preoperatively for
673 analgesia.
674 After securing the mice in a stereotaxic frame (RWD life science, Model 68528), 0.25% bupi-
675 vacaine was locally injected at the incision sites for perioperative analgesia, and ophthalmic
676 ointment was applied to protect the cornea. A midline incision was made to expose the skull,
677 which was cleaned with 2% hydrogen peroxide using sterile cotton swabs to remove connec-
678 tive tissue. The skull surface was leveled to a stereotaxic plane, and the bregma was identi-
679 fied and marked. Once dry, the exposed skull was coated with a light-curing self-etch adhe-
680 sive (3M ESPE Single Bond Universal).
681 For cerebellar electrical stimulation experiments, two small holes separated by 1.5 mm were
682 drilled in the skull above the fourth/fifth cerebellar lobules [anterior-posterior (AP), -6.25 mm;
683 medial-lateral (ML), ±0.75 mm; dorsal-ventral (DV), -1.0 mm from the dura]. Two metal elec-
684 trodes (100 μm in diameter; California Fine Wire Company, M426550) were implanted and se-
685 cured with dental cement.

686 For cortical electrical stimulation and EEG recording, two small craniotomies (~0.6 mm in di-
687 ameter) were made over the left sensory cortex (AP -0.8 mm; ML 1.5 mm) and visual cortex
688 (AP -3.5 mm, ML 1.5 mm) for the insertion of bipolar stimulation electrodes (180 μm in diame-
689 ter), which were implanted to a depth of -0.6 mm from the dura. Stainless steel screws were
690 used as EEG electrodes: one was implanted into the right visual cortex (AP -2.25 mm, ML -
691 1.5 mm), and the second into the right cerebellar vermis to serve as the reference. An addi-
692 tional screw was placed in the left cerebellar hemisphere as the ground. The electrodes and a
693 custom-made head plate were affixed to the skull using dental cement.
694 Post-operatively, meloxicam (5 mg/kg, subcutaneously) was administered once daily for 3
695 consecutive days. Mice were allowed to recover for one week prior to electrical stimulation.
696 **Cerebellar electrical stimulation and behavior assessment**
697 Before cerebellar electrical stimulation, mice were habituated to the head-fixed platform for 30
698 minutes per day over three consecutive days. Electrical stimulation (300 μA, 60 Hz, 1-ms
699 pulse width, 2 s duration) was delivered to the cerebellar cortex through a stimulus isolator
700 (AMPI, ISO Flex) driven by a Master-8 stimulator. Mouse behavior was recorded with a video
701 camera at a frame rate of 30 frames per second for 10 minutes.
702 Dystonia in mice were defined by the presence of one or more of the following abnormal pos-
703 tures or movements: prolonged forelimb elevation; persistent backward extension of the ears,
704 tightly apposed to the head; an elongated trunk posture with the abdomen close to the ground
705 and prolonged elevation or excessive extension of hindlimbs.
706 **Electrostimulation and EEG recording in the cerebral cortex**
707 One week after surgery, mice were habituated to a custom-built head plate holder for 30
708 minutes per day over three consecutive days prior to testing.
709 For stimulation experiments, the pre-implanted electrodes were connected to a stimulus isola-
710 tor (AMPI, ISO Flex). Electrical pulses (1 ms pulse width, 60 Hz frequency, 2 s duration) were
711 delivered through the isolator and controlled via TTL signals from a pulse generator (RWD life
712 science, R820). EEG signals (bandpass: 1-300 Hz) were amplified 1000-fold using an AC/DC
713 differential amplifier (A-M Systems, Model 3000), digitized at 1 kHz with a Digidata (Molecular
714 Devices, 1332A), and acquired using Clampex software (Molecular Devices, v10.7).
715 To assess cortical resilience in *Prrt2*-mutant versus wild-type mice, a stimulus-response

716 protocol was employed using progressively increasing current intensities (0, 20, 40, 80, 120,
717 160, 200, 240, 280, 320 μA). Each stimulation was separated by a 24-hour interval. The stim-
718 ulation threshold was defined as the lowest current intensity that induced after-discharges
719 (lasting ≥ 2 seconds) in the EEG trace. Each EEG recording lasted for 5 minutes, with electri-
720 cal stimulation delivered immediately following a 1-minute baseline period.

721 **Statistics**

722 All grouped data are presented as mean ± standard error of the mean (s.e.m) unless other-
723 wise stated. Statistical analyses were performed using Graphpad Prism 8 (GraphPad Soft-
724 ware Inc, La Jolla, US). No statistical methods were used to pre-determine the sample sizes.
725 The D'Agostino-Pearson omnibus (K2) test was used to assess normality.
726 Two-tailed, unpaired Student's *t*-tests were applied in Figures 7B and 7D. A two-tailed, paired
727 Student's *t*-test was used in Figures 6D-F and Figure 7-figure supplement 1B. Two-tailed, un-
728 paired Mann-Whitney test was applied in Figure 7H. Two-way ANOVAs were conducted for
729 comparisons in Figures 1C-D, 1F-G, 2B-C, 2E-F, 3C-D, 3F-G, 4B-E, 4G-J, 7I, Figure 1-figure
730 supplement 1B-C, Figure 3-figure supplement 1C-D, and Figure 7-figure supplement 2B-C. If
731 necessary, the Geisser-Greenhouse correction was applied to adjust for violations of spheric-
732 ity.
733 Statistical tests and sample sizes (including number of cells, slices, or animals) are stated in
734 the figure legends. No data were excluded from analyses. Asterisks in figures denote signifi-
735 cance levels: *P < 0.05, **P < 0.01, ***P < 0.001, ****P < 0.0001, n.s., not significant.
736 Co-immunoprecipitation assays were independently repeated at least three times in both *in*
737 *vitro* and *in vivo* tests. All attempts at replicating experiments presented in the manuscript
738 have obtained consistent conclusions.
739 Electrophysiological recordings were conducted with the experimenter blinded to group iden-
740 tity (transfected condition or animal genotype).

741 **Acknowledgements**

742 The authors thank Fei Dong, Ting-Bin Ma, Xi Zhou, Wen Zhang, Wei Ke, Yue-Jie Xiao and
743 Xue-Qin Jin for technical support for electrophysiological recording. We thank Huai-Zong
744 Shen, Zhang-Qiang Li, Xue-Jing Li and Shu-Jia Zhu for experimental support for protein ex-
745 pression. We thank Tong-Zhou Li, Hong Zhang, Jun-Jun Liu and Hai-Yan Zhen from ICE

Bioscience for experimental support in sodium current recording. We appreciate the staff at the Core Facilities for their generous technical support, and members of Xiong Lab for technical support and insightful discussions.

This work was supported by Innovation of Science and Technology 2030-Major Project “platform of nonhuman primate models", grant 2021ZD0200900 (Z.-Q.X.); National Natural Science Foundation of China, grants 82271269 (B.L.) and 82021001 (Z.-Q.X.); and Shanghai Municipal Science and Technology Major Project (Z.-Q.X.).

Additional information

Materials availability

All plasmids and mice generated in this study are available from the lead contact with a completed materials transfer agreement.

Data and code availability

The data supporting the findings of this study are included in the main text. This paper does not report the original code.

Contributions

Z.-Q.X. and B.L. conceived the study and designed the experiments. B.L., Q.-W.X. and J.Z. carried out cellular and molecular experiments and data analyses. X.-M.W., J.-Y.H. and J.-Q.P. performed animal experiments and data analyses. L.Z., J.Z., K.-X.L. and Z.-Y.W. contributed to plasmid construction. G.Y. was responsible for the knock-in mice generation. Y.-X.Z. helped with animal surgery and behavior analyses. B.L. wrote the manuscript. Q.-W.X., J.Z., X.-M.W., J.-Y.H. and Z.-Y.W. carried out manuscript review and editing. Z.-Q.X. and B.L. carried out project supervision, data interpretation and funding acquisition.

Competing interests

The authors declare no competing interests.

Supplemental information

Figure 1-figure supplement 1, Figure 2-figure supplement 1, Figure 3-figure supplement 1, Figure 6-figure supplement 1, Figure 7-figure supplement 1 and Figure 7-figure supplement 2.

774 **References**

775 Armstrong, C. M., & Bezanilla, F. (1977). Inactivation of the sodium channel. II. Gating current
776 experiments. *J Gen Physiol, 70*(5), 567-590. doi:10.1085/jgp.70.5.567
777 Balser, J. R., Nuss, H. B., Chiamvimonvat, N., Perez-Garcia, M. T., Marban, E., & Tomaselli,
778 G. F. (1996). External pore residue mediates slow inactivation in mu 1 rat skeletal
779 muscle sodium channels. *J Physiol, 494 (Pt 2)*(Pt 2), 431-442.
780 doi:10.1113/jphysiol.1996.sp021503
781 Bar-Yehuda, D., & Korngreen, A. (2008). Space-clamp problems when voltage clamping
782 neurons expressing voltage-gated conductances. *J Neurophysiol, 99*(3), 1127-1136.
783 doi:10.1152/jn.01232.2007
784 Bendahhou, S., Cummins, T. R., Kula, R. W., Fu, Y. H., & Ptacek, L. J. (2002). Impairment of
785 slow inactivation as a common mechanism for periodic paralysis in DIIS4-S5.
786 *Neurology, 58*(8), 1266-1272. doi:10.1212/wnl.58.8.1266
787 Bezanilla, F., & Armstrong, C. M. (1977). Inactivation of the sodium channel. I. Sodium current
788 experiments. *J Gen Physiol, 70*(5), 549-566. doi:10.1085/jgp.70.5.549
789 Binda, F., Valente, P., Marte, A., Baldelli, P., & Benfenati, F. (2021). Increased responsiveness
790 at the cerebellar input stage in the PRRT2 knockout model of paroxysmal kinesigenic
791 dyskinesia. *Neurobiol Dis, 152*, 105275. doi:10.1016/j.nbd.2021.105275
792 Blume, W. T., Jones, D. C., & Pathak, P. (2004). Properties of after-discharges from cortical
793 electrical stimulation in focal epilepsies. *Clin Neurophysiol, 115*(4), 982-989.
794 doi:10.1016/j.clinph.2003.11.023
795 Cannon, S. C. (2018). Sodium Channelopathies of Skeletal Muscle. *Handb Exp Pharmacol,*
796 *246*, 309-330. doi:10.1007/164_2017_52
797 Catterall, W. A. (2023). Voltage gated sodium and calcium channels: Discovery, structure,
798 function, and Pharmacology. *Channels (Austin), 17*(1), 2281714.
799 doi:10.1080/19336950.2023.2281714
800 Catterall, W. A., Gamal El-Din, T. M., & Wisedchaisri, G. (2024). The chemistry of electrical
801 signaling in sodium channels from bacteria and beyond. *Cell Chem Biol, 31*(8), 1405-
802 1421. doi:10.1016/j.chembiol.2024.07.010
803 Catterall, W. A., Goldin, A. L., & Waxman, S. G. (2005). International Union of Pharmacology.
804 XLVII. Nomenclature and structure-function relationships of voltage-gated sodium
805 channels. *Pharmacol Rev, 57*(4), 397-409. doi:10.1124/pr.57.4.4
806 Catterall, W. A., Wisedchaisri, G., & Zheng, N. (2020). The conformational cycle of a
807 prototypical voltage-gated sodium channel. *Nat Chem Biol, 16*(12), 1314-1320.
808 doi:10.1038/s41589-020-0644-4
809 Chancey, J. H., Shockett, P. E., & O'Reilly, J. P. (2007). Relative resistance to slow
810 inactivation of human cardiac Na+ channel hNav1.5 is reversed by lysine or
811 glutamine substitution at V930 in D2-S6. *Am J Physiol Cell Physiol, 293*(6), C1895-
812 1905. doi:10.1152/ajpcell.00377.2007

813 Chatterjee, S., Vyas, R., Chalamalasetti, S. V., Sahu, I. D., Clatot, J., Wan, X., . . .
814 Chakrapani, S. (2018). The voltage-gated sodium channel pore exhibits
815 conformational flexibility during slow inactivation. *J Gen Physiol, 150*(9), 1333-1347.
816 doi:10.1085/jgp.201812118
817 Chen, W. J., Lin, Y., Xiong, Z. Q., Wei, W., Ni, W., Tan, G. H., . . . Wu, Z. Y. (2011). Exome
818 sequencing identifies truncating mutations in PRRT2 that cause paroxysmal
819 kinesigenic dyskinesia. *Nat Genet, 43*(12), 1252-1255. doi:10.1038/ng.1008
820 Chen, Y., Yu, F. H., Surmeier, D. J., Scheuer, T., & Catterall, W. A. (2006). Neuromodulation of
821 Na+ channel slow inactivation via cAMP-dependent protein kinase and protein kinase
822 C. *Neuron, 49*(3), 409-420. doi:10.1016/j.neuron.2006.01.009
823 Coleman, J., Jouannot, O., Ramakrishnan, S. K., Zanetti, M. N., Wang, J., Salpietro, V., . . .
824 Krishnakumar, S. S. (2018). PRRT2 Regulates Synaptic Fusion by Directly
825 Modulating SNARE Complex Assembly. *Cell Rep, 22*(3), 820-831.
826 doi:10.1016/j.celrep.2017.12.056
827 Cummins, T. R., & Sigworth, F. J. (1996). Impaired slow inactivation in mutant sodium
828 channels. *Biophys J, 71*(1), 227-236. doi:10.1016/S0006-3495(96)79219-6
829 Cusdin, F. S., Clare, J. J., & Jackson, A. P. (2008). Trafficking and cellular distribution of
830 voltage-gated sodium channels. *Traffic, 9*(1), 17-26. doi:10.1111/j.1600-
831 0854.2007.00673.x
832 Dib-Hajj, S. D., Geha, P., & Waxman, S. G. (2017). Sodium channels in pain disorders:
833 pathophysiology and prospects for treatment. *Pain, 158 Suppl 1*(Suppl 1), S97-S107.
834 doi:10.1097/j.pain.0000000000000854
835 Dover, K., Solinas, S., D'Angelo, E., & Goldfarb, M. (2010). Long-term inactivation particle for
836 voltage-gated sodium channels. *J Physiol, 588*(Pt 19), 3695-3711.
837 doi:10.1113/jphysiol.2010.192559
838 Ehrlich, K. C., Lacey, M., & Ehrlich, M. (2020). Epigenetics of Skeletal Muscle-Associated
839 Genes in the ASB, LRRC, TMEM, and OSBPL Gene Families. *Epigenomes, 4*(1).
840 doi:10.3390/epigenomes4010001
841 Escayg, A., & Goldin, A. L. (2010). Sodium channel SCN1A and epilepsy: mutations and
842 mechanisms. *Epilepsia, 51*(9), 1650-1658. doi:10.1111/j.1528-1167.2010.02640.x
843 Featherstone, D. E., Richmond, J. E., & Ruben, P. C. (1996). Interaction between fast and
844 slow inactivation in Skm1 sodium channels. *Biophys J, 71*(6), 3098-3109.
845 doi:10.1016/S0006-3495(96)79504-8
846 Ferrante, D., Sterlini, B., Prestigio, C., Marte, A., Corradi, A., Onofri, F., . . . Baldelli, P. (2021).
847 PRRT2 modulates presynaptic Ca(2+) influx by interacting with P/Q-type channels.
848 *Cell Rep, 35*(11), 109248. doi:10.1016/j.celrep.2021.109248
849 Fleidervish, I. A., Friedman, A., & Gutnick, M. J. (1996). Slow inactivation of Na+ current and
850 slow cumulative spike adaptation in mouse and guinea-pig neocortical neurones in
851 slices. *J Physiol, 493 (Pt 1)*, 83-97. doi:10.1113/jphysiol.1996.sp021366

852 Franchi, F., Marte, A., Corradi, B., Sterlini, B., Alberini, G., Romei, A., . . . Benfenati, F. (2023).
853 The intramembrane COOH-terminal domain of PRRT2 regulates voltage-dependent
854 Na(+) channels. *J Biol Chem*, 104632. doi:10.1016/j.jbc.2023.104632
855 Freal, A., Jamann, N., Ten Bos, J., Jansen, J., Petersen, N., Ligthart, T., . . . Kole, M. H. P.
856 (2023). Sodium channel endocytosis drives axon initial segment plasticity. *Sci Adv,*
857 *9*(37), eadf3885. doi:10.1126/sciadv.adf3885
858 Fruscione, F., Valente, P., Sterlini, B., Romei, A., Baldassari, S., Fadda, M., . . . Benfenati, F.
859 (2018). PRRT2 controls neuronal excitability by negatively modulating Na^+ channel
860 1.2/1.6 activity. *Brain, 141*(4), 1000-1016. doi:10.1093/brain/awy051
861 Gade, A. R., Marx, S. O., & Pitt, G. S. (2020). An interaction between the III-IV linker and CTD
862 in NaV1.5 confers regulation of inactivation by CaM and FHF. *J Gen Physiol, 152*(2).
863 doi:10.1085/jgp.201912434
864 Ganguly, S., Thompson, C. H., & George, A. L., Jr. (2021). Enhanced slow inactivation
865 contributes to dysfunction of a recurrent SCN2A mutation associated with
866 developmental and epileptic encephalopathy. *J Physiol, 599*(18), 4375-4388.
867 doi:10.1113/JP281834
868 Ghovanloo, M. R., Effraim, P. R., Yuan, J. H., Schulman, B. R., Jacobs, D. S., Dib-Hajj, S. D.,
869 & Waxman, S. G. (2023). Nav1.7 P610T mutation in two siblings with persistent
870 ocular pain after corneal axon transection: impaired slow inactivation and
871 hyperexcitable trigeminal neurons. *J Neurophysiol, 129*(3), 609-618.
872 doi:10.1152/jn.00457.2022
873 Goetz, R., Dover, K., Laezza, F., Shtraizent, N., Huang, X., Tchetchik, D., . . . Mohammadi, M.
874 (2009). Crystal structure of a fibroblast growth factor homologous factor (FHF)
875 defines a conserved surface on FHFs for binding and modulation of voltage-gated
876 sodium channels. *J Biol Chem, 284*(26), 17883-17896. doi:10.1074/jbc.M109.001842
877 Goldin, A. L. (2001). Resurgence of sodium channel research. *Annu Rev Physiol, 63*, 871-
878 894. doi:10.1146/annurev.physiol.63.1.871
879 Goldin, A. L. (2003). Mechanisms of sodium channel inactivation. *Curr Opin Neurobiol, 13*(3),
880 284-290. doi:10.1016/s0959-4388(03)00065-5
881 Hayward, L. J., Sandoval, G. M., & Cannon, S. C. (1999). Defective slow inactivation of
882 sodium channels contributes to familial periodic paralysis. *Neurology, 52*(7), 1447-
883 1453. doi:10.1212/wnl.52.7.1447
884 He, B., & Soderlund, D. M. (2014). Functional expression of Rat Nav1.6 voltage-gated sodium
885 channels in HEK293 cells: modulation by the auxiliary beta1 subunit. *PLoS One, 9*(1),
886 e85188. doi:10.1371/journal.pone.0085188
887 Hedrich, U. B. S., Lauxmann, S., & Lerche, H. (2019). SCN2A channelopathies: Mechanisms
888 and models. *Epilepsia, 60 Suppl 3*, S68-S76. doi:10.1111/epi.14731
889 Higerd-Rusli, G. P., Tyagi, S., Liu, S., Dib-Hajj, F. B., Waxman, S. G., & Dib-Hajj, S. D. (2023).
890 The fates of internalized Na(V)1.7 channels in sensory neurons: Retrograde

891 cotransport with other ion channels, axon-specific recycling, and degradation. *J Biol*
892 *Chem, 299*(1), 102816. doi:10.1016/j.jbc.2022.102816
893 Hodgkin, A. L., & Huxley, A. F. (1952). A quantitative description of membrane current and its
894 application to conduction and excitation in nerve. *J Physiol, 117*(4), 500-544.
895 doi:10.1113/jphysiol.1952.sp004764
896 Hu, W., & Shu, Y. (2012). Axonal bleb recording. *Neurosci Bull, 28*(4), 342-350.
897 doi:10.1007/s12264-012-1247-1
898 Isom, L. L., De Jongh, K. S., Patton, D. E., Reber, B. F., Offord, J., Charbonneau, H., . . .
899 Catterall, W. A. (1992). Primary structure and functional expression of the beta 1
900 subunit of the rat brain sodium channel. *Science, 256*(5058), 839-842.
901 doi:10.1126/science.1375395
902 Jiang, D., Shi, H., Tonggu, L., Gamal El-Din, T. M., Lenaeus, M. J., Zhao, Y., . . . Catterall, W.
903 A. (2020). Structure of the Cardiac Sodium Channel. *Cell, 180*(1), 122-134 e110.
904 doi:10.1016/j.cell.2019.11.041
905 Kim, E., Owen, B., Holmes, W. R., & Grover, L. M. (2012). Decreased afferent excitability
906 contributes to synaptic depression during high-frequency stimulation in hippocampal
907 area CA1. *J Neurophysiol, 108*(7), 1965-1976. doi:10.1152/jn.00276.2011
908 Lee, H. Y., Huang, Y., Bruneau, N., Roll, P., Roberson, E. D., Hermann, M., . . . Ptacek, L. J.
909 (2012). Mutations in the gene PRRT2 cause paroxysmal kinesigenic dyskinesia with
910 infantile convulsions. *Cell Rep, 1*(1), 2-12. doi:10.1016/j.celrep.2011.11.001
911 Liu, H., Wang, H. G., Pitt, G., & Liu, Z. (2022). Direct Observation of Compartment-Specific
912 Localization and Dynamics of Voltage-Gated Sodium Channels. *J Neurosci, 42*(28),
913 5482-5498. doi:10.1523/JNEUROSCI.0086-22.2022
914 Lu, B., Lou, S. S., Xu, R. S., Kong, D. L., Wu, R. J., Zhang, J., . . . Xiong, Z. Q. (2021).
915 Cerebellar spreading depolarization mediates paroxysmal movement disorder. *Cell*
916 *Rep, 36*(12), 109743. doi:10.1016/j.celrep.2021.109743
917 Makita, N., Bennett, P. B., & George, A. L., Jr. (1996). Molecular determinants of beta 1
918 subunit-induced gating modulation in voltage-dependent Na+ channels. *J Neurosci,*
919 *16*(22), 7117-7127. doi:10.1523/JNEUROSCI.16-22-07117.1996
920 Mantegazza, M., Cestele, S., & Catterall, W. A. (2021). Sodium channelopathies of skeletal
921 muscle and brain. *Physiol Rev, 101*(4), 1633-1689. doi:10.1152/physrev.00025.2020
922 Matsuda, T., & Cepko, C. L. (2004). Electroporation and RNA interference in the rodent retina
923 in vivo and in vitro. *Proc Natl Acad Sci U S A, 101*(1), 16-22.
924 doi:10.1073/pnas.2235688100
925 Meisler, M. H., Hill, S. F., & Yu, W. (2021). Sodium channelopathies in neurodevelopmental
926 disorders. *Nat Rev Neurosci, 22*(3), 152-166. doi:10.1038/s41583-020-00418-4
927 Mickus, T., Jung, H. Y., & Spruston, N. (1999). Slow sodium channel inactivation in CA1
928 pyramidal cells. *Ann N Y Acad Sci, 868*, 97-101. doi:10.1111/j.1749-
929 6632.1999.tb11280.x

930 Misra, S. N., Kahlig, K. M., & George, A. L., Jr. (2008). Impaired NaV1.2 function and reduced
931 cell surface expression in benign familial neonatal-infantile seizures. *Epilepsia, 49*(9),
932 1535-1545. doi:10.1111/j.1528-1167.2008.01619.x
933 Mitrovic, N., George, A. L., Jr., & Horn, R. (2000). Role of domain 4 in sodium channel slow
934 inactivation. *J Gen Physiol, 115*(6), 707-718. doi:10.1085/jgp.115.6.707
935 Noreng, S., Li, T., & Payandeh, J. (2021). Structural Pharmacology of Voltage-Gated Sodium
936 Channels. *J Mol Biol, 433*(17), 166967. doi:10.1016/j.jmb.2021.166967
937 Olsen, S. K., Garbi, M., Zampieri, N., Eliseenkova, A. V., Ornitz, D. M., Goldfarb, M., &
938 Mohammadi, M. (2003). Fibroblast growth factor (FGF) homologous factors share
939 structural but not functional homology with FGFs. *J Biol Chem, 278*(36), 34226-
940 34236. doi:10.1074/jbc.M303183200
941 Oort, P. J., Warden, C. H., Baumann, T. K., Knotts, T. A., & Adams, S. H. (2007).
942 Characterization of Tusc5, an adipocyte gene co-expressed in peripheral neurons.
943 *Mol Cell Endocrinol, 276*(1-2), 24-35. doi:10.1016/j.mce.2007.06.005
944 Pan, X., Li, Z., Huang, X., Huang, G., Gao, S., Shen, H., . . . Yan, N. (2019). Molecular basis
945 for pore blockade of human Na(+) channel Na(v)1.2 by the mu-conotoxin KIIIA.
946 *Science, 363*(6433), 1309-1313. doi:10.1126/science.aaw2999
947 Pan, X., Li, Z., Jin, X., Zhao, Y., Huang, G., Huang, X., . . . Yan, N. (2021). Comparative
948 structural analysis of human Na(v)1.1 and Na(v)1.5 reveals mutational hotspots for
949 sodium channelopathies. *Proc Natl Acad Sci U S A, 118*(11).
950 doi:10.1073/pnas.2100066118
951 Payandeh, J. (2018). Progress in understanding slow inactivation speeds up. *J Gen Physiol,*
952 *150*(9), 1235-1238. doi:10.1085/jgp.201812149
953 Remme, C. A. (2013). Cardiac sodium channelopathy associated with SCN5A mutations:
954 electrophysiological, molecular and genetic aspects. *J Physiol, 591*(17), 4099-4116.
955 doi:10.1113/jphysiol.2013.256461
956 Riant, F., Roos, C., Roubertie, A., Barbance, C., Hadjadj, J., Auvin, S., . . . Ducros, A. (2022).
957 Hemiplegic Migraine Associated With PRRT2 Variations: A Clinical and Genetic
958 Study. *Neurology, 98*(1), e51-e61. doi:10.1212/WNL.0000000000012947
959 Richmond, J. E., Featherstone, D. E., Hartmann, H. A., & Ruben, P. C. (1998). Slow
960 inactivation in human cardiac sodium channels. *Biophys J, 74*(6), 2945-2952.
961 doi:10.1016/S0006-3495(98)78001-4
962 Rudy, B. (1978). Slow inactivation of the sodium conductance in squid giant axons. Pronase
963 resistance. *J Physiol, 283*, 1-21. doi:10.1113/jphysiol.1978.sp012485
964 Sallman Almen, M., Bringeland, N., Fredriksson, R., & Schioth, H. B. (2012). The dispanins: a
965 novel gene family of ancient origin that contains 14 human members. *PLoS One,*
966 *7*(2), e31961. doi:10.1371/journal.pone.0031961
967 Santana-Varela, S., Bogdanov, Y. D., Gossage, S. J., Okorokov, A. L., Li, S., de Clauser,
968 L., . . . Cox, J. J. (2021). Tools for analysis and conditional deletion of subsets of

969 sensory neurons. *Wellcome Open Res, 6*, 250.
970 doi:10.12688/wellcomeopenres.17090.1
971 Shibata, T., Koide, H., Hayashi, R., Nagata, K., Takeo, C., Yoshida, T., . . . Tatsuno, I. (2007).
972 Molecular cloning and characterization of rat brain endothelial cell derived gene-1
973 (tumor suppressor candidate 5) expressing abundantly in adipose tissues. *Mol Cell*
974 *Endocrinol, 263*(1-2), 38-45. doi:10.1016/j.mce.2006.08.007
975 Silva, J. (2014). Slow inactivation of Na(+) channels. *Handb Exp Pharmacol, 221*, 33-49.
976 doi:10.1007/978-3-642-41588-3_3
977 Tan, G. H., Liu, Y. Y., Wang, L., Li, K., Zhang, Z. Q., Li, H. F., . . . Xiong, Z. Q. (2018). PRRT2
978 deficiency induces paroxysmal kinesigenic dyskinesia by regulating synaptic
979 transmission in cerebellum. *Cell Res, 28*(1), 90-110. doi:10.1038/cr.2017.128
980 Thompson, C. H., Potet, F., Abramova, T. V., DeKeyser, J. M., Ghabra, N. F., Vanoye, C.
981 G., . . . George, A. L. (2023). Epilepsy-associated SCN2A (NaV1.2) variants exhibit
982 diverse and complex functional properties. *J Gen Physiol, 155*(10).
983 doi:10.1085/jgp.202313375
984 Todt, H., Dudley, S. C., Jr., Kyle, J. W., French, R. J., & Fozzard, H. A. (1999). Ultra-slow
985 inactivation in mu1 Na+ channels is produced by a structural rearrangement of the
986 outer vestibule. *Biophys J, 76*(3), 1335-1345. doi:10.1016/S0006-3495(99)77296-6
987 Tyagi, S., Higerd-Rusli, G. P., Akin, E. J., Waxman, S. G., & Dib-Hajj, S. D. (2025). Sculpting
988 excitable membranes: voltage-gated ion channel delivery and distribution. *Nat Rev*
989 *Neurosci, 26*(6), 313-332. doi:10.1038/s41583-025-00917-2
990 Ulbricht, W. (1977). Ionic channels and gating currents in excitable membranes. *Annu Rev*
991 *Biophys Bioeng, 6*, 7-31. doi:10.1146/annurev.bb.06.060177.000255
992 Valente, P., Castroflorio, E., Rossi, P., Fadda, M., Sterlini, B., Cervigni, R. I., . . . Benfenati, F.
993 (2016). PRRT2 Is a Key Component of the Ca(2+)-Dependent Neurotransmitter
994 Release Machinery. *Cell Rep, 15*(1), 117-131. doi:10.1016/j.celrep.2016.03.005
995 Valente, P., Marte, A., Franchi, F., Sterlini, B., Casagrande, S., Corradi, A., . . . Benfenati, F.
996 (2023). A Push-Pull Mechanism Between PRRT2 and beta4-subunit Differentially
997 Regulates Membrane Exposure and Biophysical Properties of NaV1.2 Sodium
998 Channels. *Mol Neurobiol, 60*(3), 1281-1296. doi:10.1007/s12035-022-03112-x
999 Venkatesan, K., Liu, Y., & Goldfarb, M. (2014). Fast-onset long-term open-state block of
1000 sodium channels by A-type FHFs mediates classical spike accommodation in
1001 hippocampal pyramidal neurons. *J Neurosci, 34*(48), 16126-16139.
1002 doi:10.1523/JNEUROSCI.1271-14.2014
1003 Vilin, Y. Y., Makita, N., George, A. L., Jr., & Ruben, P. C. (1999). Structural determinants of
1004 slow inactivation in human cardiac and skeletal muscle sodium channels. *Biophys J,*
1005 *77*(3), 1384-1393. doi:10.1016/S0006-3495(99)76987-0
1006 Vilin, Y. Y., & Ruben, P. C. (2001). Slow inactivation in voltage-gated sodium channels:
1007 molecular substrates and contributions to channelopathies. *Cell Biochem Biophys,*

1008 *35*(2), 171-190. doi:10.1385/CBB:35:2:171
1009 Wallner, M., Weigl, L., Meera, P., & Lotan, I. (1993). Modulation of the skeletal muscle sodium
1010 channel alpha-subunit by the beta 1-subunit. *FEBS Lett, 336*(3), 535-539.
1011 doi:10.1016/0014-5793(93)80871-q
1012 Wang, D. W., Makita, N., Kitabatake, A., Balser, J. R., & George, A. L., Jr. (2000). Enhanced
1013 Na(+) channel intermediate inactivation in Brugada syndrome. *Circ Res, 87*(8), E37-
1014 43. doi:10.1161/01.res.87.8.e37
1015 Wang, J. L., Cao, L., Li, X. H., Hu, Z. M., Li, J. D., Zhang, J. G., . . . Tang, B. S. (2011).
1016 Identification of PRRT2 as the causative gene of paroxysmal kinesigenic dyskinesias.
1017 *Brain, 134*(Pt 12), 3493-3501. doi:10.1093/brain/awr289
1018 Wang, S. Y., & Wang, G. K. (1997). A mutation in segment I-S6 alters slow inactivation of
1019 sodium channels. *Biophys J, 72*(4), 1633-1640. doi:10.1016/S0006-3495(97)78809-X
1020 Waxman, S. G. (2013). Painful Na-channelopathies: an expanding universe. *Trends Mol Med,*
1021 *19*(7), 406-409. doi:10.1016/j.molmed.2013.04.003
1022 Webb, J., Wu, F. F., & Cannon, S. C. (2009). Slow inactivation of the NaV1.4 sodium channel
1023 in mammalian cells is impeded by co-expression of the beta1 subunit. *Pflugers Arch,*
1024 *457*(6), 1253-1263. doi:10.1007/s00424-008-0600-8
1025 Wisedchaisri, G., & Gamal El-Din, T. M. (2022). Druggability of Voltage-Gated Sodium
1026 Channels-Exploring Old and New Drug Receptor Sites. *Front Pharmacol, 13*, 858348.
1027 doi:10.3389/fphar.2022.858348
1028 Wu, X. M., Lu, B., He, J. Y., Zhang, Y. X., Wu, Z. Y., & Xiong, Z. Q. (2025). Aberrant outputs of
1029 glutamatergic neurons in deep cerebellar nuclei mediate dystonic movements. *Sci*
1030 *Adv, 11*(19), eadp2377. doi:10.1126/sciadv.adp2377
1031 Xiong, W., Farukhi, Y. Z., Tian, Y., Disilvestre, D., Li, R. A., & Tomaselli, G. F. (2006). A
1032 conserved ring of charge in mammalian Na+ channels: a molecular regulator of the
1033 outer pore conformation during slow inactivation. *J Physiol, 576*(Pt 3), 739-754.
1034 doi:10.1113/jphysiol.2006.115105
1035 Xu, R., Thomas, E. A., Gazina, E. V., Richards, K. L., Quick, M., Wallace, R. H., . . . Petrou, S.
1036 (2007). Generalized epilepsy with febrile seizures plus-associated sodium channel
1037 beta1 subunit mutations severely reduce beta subunit-mediated modulation of sodium
1038 channel function. *Neuroscience, 148*(1), 164-174.
1039 doi:10.1016/j.neuroscience.2007.05.038
1040 Yamano, R., Miyazaki, H., & Nukina, N. (2022). The diffuse distribution of Nav1.2 on mid-
1041 axonal regions is a marker for unmyelinated fibers in the central nervous system.
1042 *Neurosci Res, 177*, 145-150. doi:10.1016/j.neures.2021.11.005
1043 Yang, H., Wang, H., & Jaenisch, R. (2014). Generating genetically modified mice using
1044 CRISPR/Cas-mediated genome engineering. *Nat Protoc, 9*(8), 1956-1968.
1045 doi:10.1038/nprot.2014.134
1046 Yu, F. H., Mantegazza, M., Westenbroek, R. E., Robbins, C. A., Kalume, F., Burton, K. A., . . .

Catterall, W. A. (2006). Reduced sodium current in GABAergic interneurons in a mouse model of severe myoclonic epilepsy in infancy. *Nat Neurosci, 9*(9), 1142-1149. doi:10.1038/nn1754

Zang, Y., Marder, E., & Marom, S. (2023). Sodium channel slow inactivation normalizes firing in axons with uneven conductance distributions. *Curr Biol, 33*(9), 1818-1824 e1813. doi:10.1016/j.cub.2023.03.043

1054 **Figures**

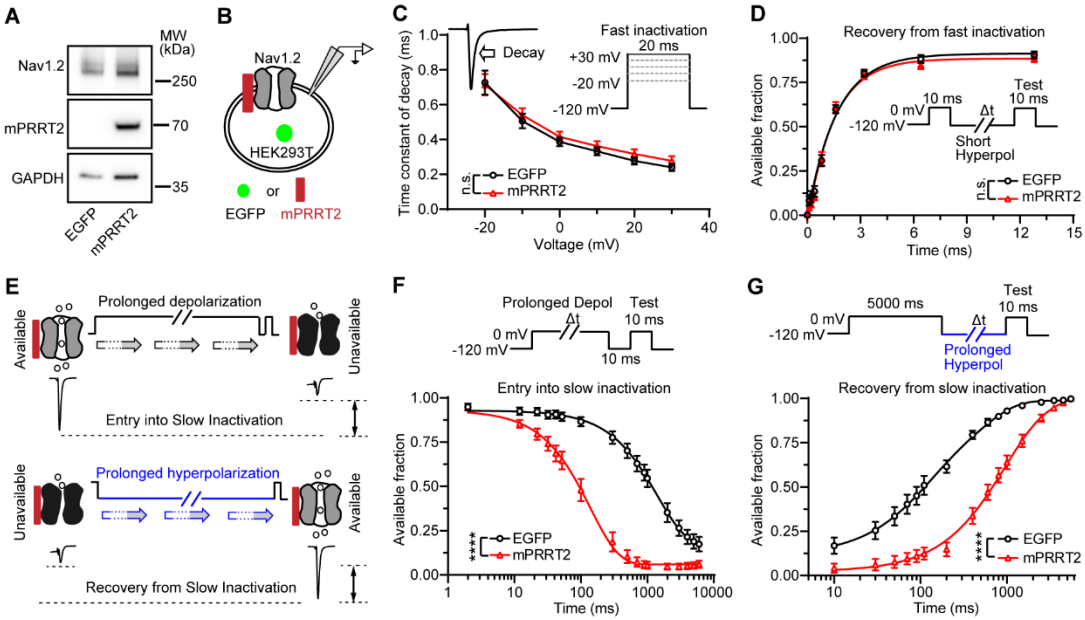

1055

1056 **Figure 1 PRRT2 regulates slow inactivation of Nav1.2 channels**

1057 **(A and B)** Representative immunoblots showing PRRT2 protein expression (A) and sche-
1058 matic of whole-cell recording (B) in Nav1.2-stably expressing HEK293T cells transfected with
1059 constructs encoding either EGFP or mouse PRRT2 (mPRRT2). MW, molecular weight.

1060 **(C)** Fast-inactivation decay time constants of sodium currents evoked by 20-ms depolarizing
1061 steps to the indicated command voltages (EGFP: *n* = 13 cells, mPRRT2: *n* = 13 cells). Insert:
1062 representative sodium current traces elicited by a brief depolarization (left) and voltage-clamp
1063 protocol used to assess fast inactivation (right). The arrow indicates the decay of the sodium
1064 current attributable to fast inactivation.

1065 **(D)** Recovery from fast inactivation of Nav1.2 channels (EGFP: *n* = 10 cells, mPRRT2: *n* = 7
1066 cells). Insert: Protocol for examining fast inactivation recovery.

1067 **(E)** Schematic diagram of entry into and recovery from slow inactivation of voltage-gated so-
1068 dium channels. Slow inactivation modulates the availability of the sodium channels.

1069 **(F)** Entry into slow-inactivated state of Nav1.2 channels induced by progressively longer de-
1070 polarization (EGFP: *n* = 6 cells, mPRRT2: *n* = 6 cells).

1071 **(G)** The effects of PRRT2 on the recovery of Nav1.2 channels from slow-inactivated state in-
1072 duced by 5-s depolarization (EGFP: *n* = 6 cells, PRRT2: *n* = 6 cells). Data are presented as
1073 mean ± s.e.m. Two-tailed, unpaired Student's *t*-test was used in C, and two-way ANOVAs
1074 were used in D, F, and G. ****$P < 0.0001$. n.s., not significant.

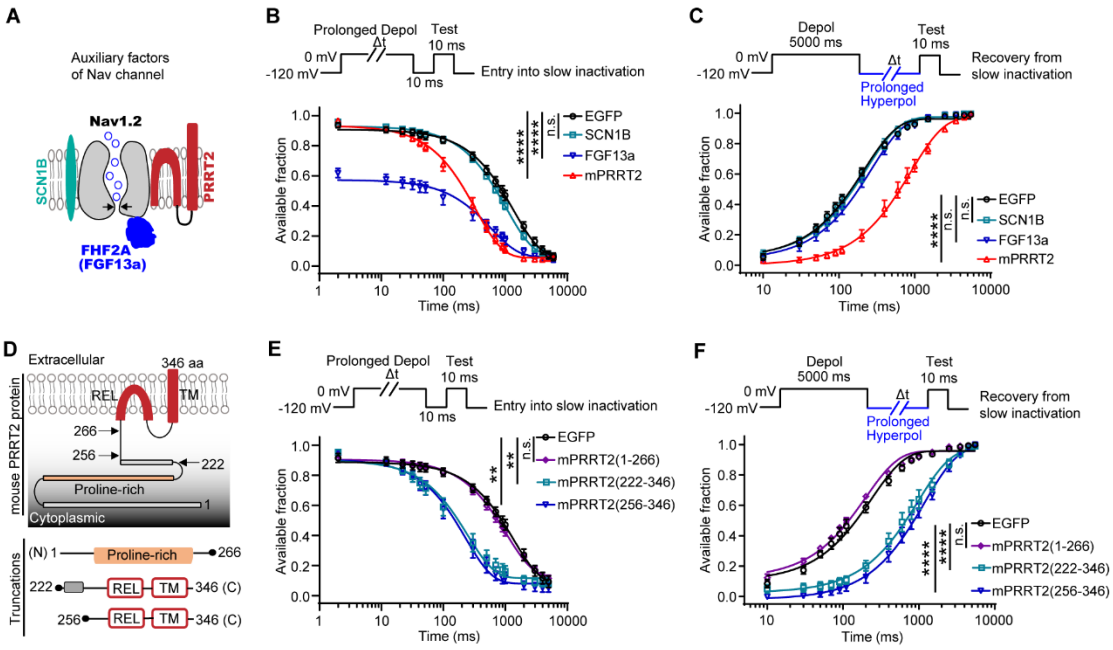

1075

1076 **Figure 2 Functional auxiliary factors in the regulation of Nav channel slow inactivation**

1077 **(A)** Diagram of Nav channel with potent auxiliary factors, encompassing SCN1B, FHF2A (also

1078 known as FGF13a) and PRRT2.

1079 **(B)** The effects of auxiliary factors on the entry of Nav1.2 channels into slow inactivation

1080 (EGFP: *n* = 12 cells, mPRRT2: *n* = 14 cells, SCN1B: *n* = 9 cells, FGF13a: *n* = 12 cells).

1081 **(C)** The effects of auxiliary factors on the recovery of Nav1.2 channels from slow-inactivated

1082 state induced by 5-s depolarization (EGFP: *n* = 12 cells, mPRRT2: *n* = 12 cells, SCN1B: *n* =

1083 12 cells, FGF13a: *n* = 12 cells).

1084 **(D)** Schematic representation of the putative topology of mouse PRRT2 and three truncations.

1085 Numbers indicate the positions of the amino acid. REL, re-entrant loop. TM, transmembrane

1086 domain. N, amino terminus. C, carboxyl terminus. aa, amino acid.

1087 **(E)** Effects of PRRT2 truncations on the entry of Nav1.2 channels into slow inactivation

1088 (EGFP: *n* = 5 cells, mPRRT2(1–266): *n* = 14 cells, mPRRT2(222–346): *n* = 12 cells,

1089 mPRRT2(256–346): *n* = 12 cells).

1090 **(F)** Effects of PRRT2 truncations on the recovery of Nav1.2 channels from slow-inactivated

1091 state induced by 5-s depolarization (EGFP: *n* = 5 cells, mPRRT2(1–266): *n* = 10 cells,

1092 mPRRT2(222–346): *n* = 10 cells, mPRRT2(256–346): *n* = 12 cells). Data are presented as

1093 mean ± s.e.m. The main effect of group was assessed using two-way ANOVAs (B, C, E and

1094 F). $^{**}P < 0.01$, $^{****}P < 0.0001$, n.s., not significant.

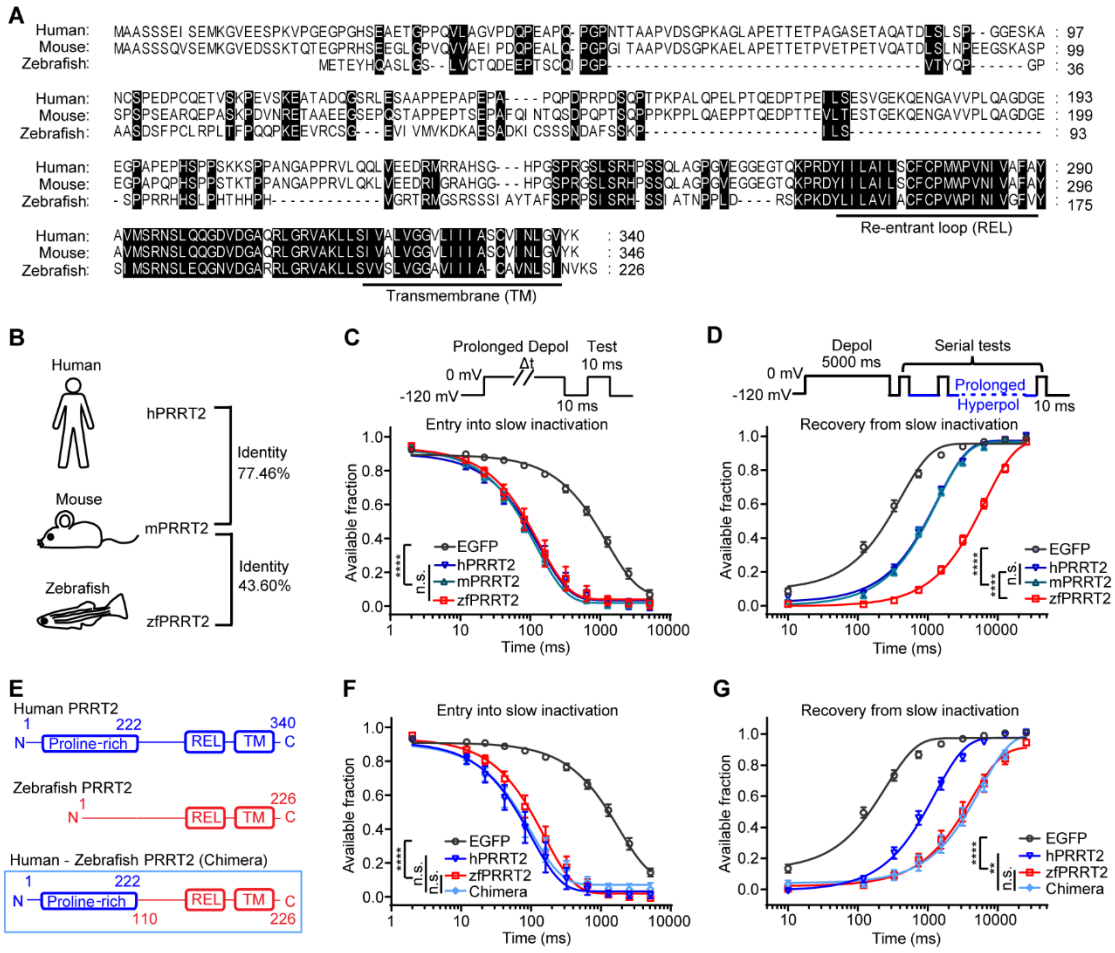

Figure 3 Evolutionarily conserved effects of PRRT2 on Nav channel slow inactivation

(A) Sequence alignment of PRRT2 protein in human, mouse and zebrafish. Conserved amino acids are highlighted and the membrane-associated domains in carboxyl terminus of PRRT2 are underlined. REL, re-entrant loop. TM, transmembrane domain.

(B) Sequence identity of PRRT2 protein in human (hPRRT2), mouse (mPRRT2) and zebrafish (zfPRRT2). Identity is calculated by using protein BLAST tool from NCBI.

(C) The effects of PRRT2 from different species on the entry of Nav1.2 channels into slow inactivation (EGFP: *n* = 16 cells, mPRRT2: *n* = 19 cells, hPRRT2: *n* = 20 cells, zfPRRT2: *n* = 11 cells).

(D) The effects of PRRT2 from different species on the recovery of Nav1.2 channels from slow-inactivated state induced by 5-s depolarization (EGFP: *n* = 16 cells, mPRRT2: *n* = 19 cells, hPRRT2: *n* = 19 cells, zfPRRT2: *n* = 11 cells).

(E) Diagram for the chimeric construct of PRRT2 originated from human and zebrafish.

(F) The effect of chimeric PRRT2 on the entry of Nav1.2 channels into slow inactivation

1110 (EGFP: *n* = 11 cells, hPRRT2: *n* = 6 cells, zfPRRT2: *n* = 10 cells, Chimera: *n* = 11 cells).

1111 **(G)** The effect of chimeric PRRT2 on the recovery of Nav1.2 channels from slow-inactivated

1112 state induced by 5-s depolarization (EGFP: *n* = 11 cells, hPRRT2: *n* = 6 cells, zfPRRT2: *n* =

1113 10 cells, Chimera: *n* = 9 cells). Data are presented as mean ± s.e.m. The main effect of group

1114 was assessed using two-way ANOVAs (C, D, F and G). $^{**}P < 0.01$, $^{****}P < 0.0001$, n.s., not

1115 significant.

1116

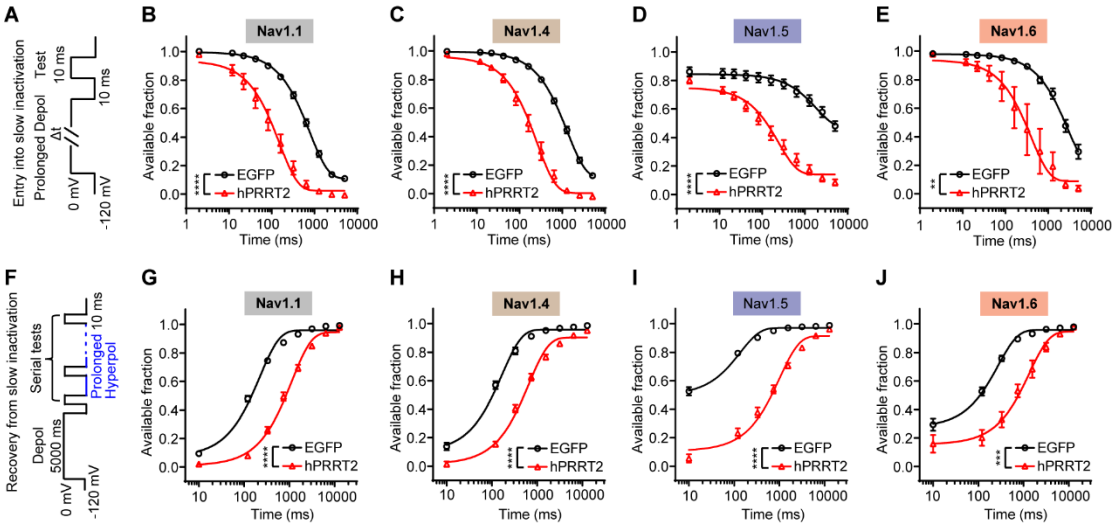

Figure 4 PRRT2 promotes slow inactivation across multiple human Nav channel isoforms

(A) Protocol for examining the entry of Nav channels into slow-inactivated state.

(B-E) The effects of human PRRT2 (hPRRT2) on the entry of Nav1.1, Nav1.4, Nav1.5 and Nav1.6 channels into slow inactivation. In (B), analyses for Nav1.1 (EGFP: *n* = 10 cells, hPRRT2: *n* = 12 cells); In (C), analyses for Nav1.4 (EGFP: *n* = 11 cells, hPRRT2: *n* = 11 cells); In (D), analyses for Nav1.5 (EGFP: *n* = 17 cells, hPRRT2: *n* = 17 cells); In (E), analyses for Nav1.6 (EGFP: *n* = 5 cells, hPRRT2: *n* = 4 cells).

(F) Protocol for examining the recovery of Nav channels from slow-inactivated state.

(G-J) The effects of human PRRT2 on the recovery of Nav1.1, Nav1.4, Nav1.5 and Nav1.6 channels from slow-inactivated state induced by 5-s depolarization. In (G), analyses for Nav1.1 (EGFP: *n* = 10 cells, hPRRT2: *n* = 12 cells); In (H), analyses for Nav1.4 (EGFP: *n* = 11 cells, hPRRT2: *n* = 11 cells); In (I), analyses for Nav1.5 (EGFP: *n* = 16 cells, hPRRT2: *n* = 15 cells); In (J), analyses for Nav1.6 (EGFP: *n* = 5 cells, hPRRT2: *n* = 4 cells)

Data are presented as mean ± s.e.m. The main effect of group was assessed using two-way ANOVAs (B-E and G-J). ***P* < 0.01, ****P* < 0.001, *****P* < 0.0001.

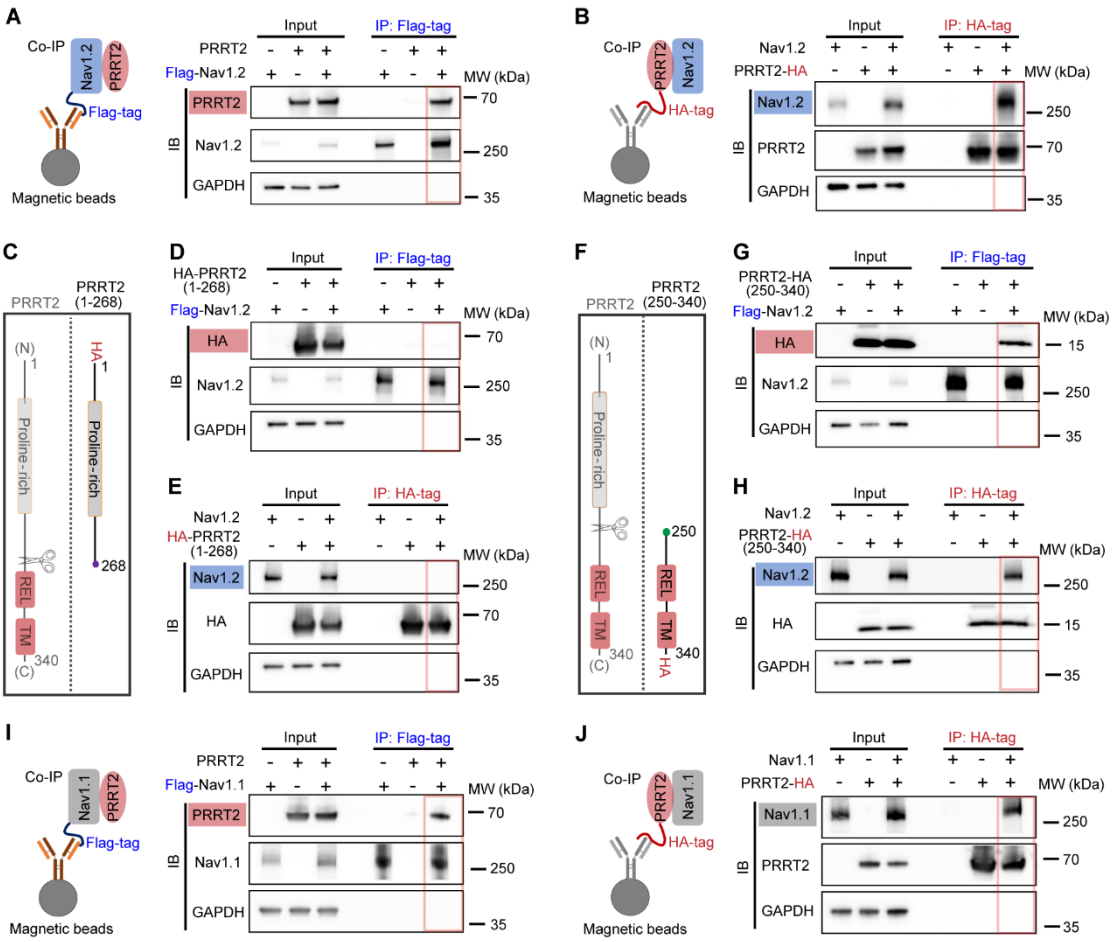

Figure 5 Association between PRRT2 and Nav channels *in vitro*

(A and B) Schematic diagram of the co-immunoprecipitation assay used to detect association between human PRRT2 and Nav1.2. Flag-tagged Nav1.2 (+), HA-tagged PRRT2 (+) and empty (-) vectors were transfected in HEK293T cells as indicated. The cell lysates were immunoprecipitated with anti-Flag (A) or anti-HA (B) magnetic beads, the captured proteins were analyzed by SDS-PAGE and immunoblotting.

(C) Diagram for HA-tagged truncation of human PRRT2 (PRRT2(1–268)), in which the carboxyl terminus of PRRT2 was deleted. REL, re-entrant loop. TM, transmembrane domain.

(D and E) Co-immunoprecipitation assay for potential association between Nav1.2 and PRRT2(1–268). The proteins immunoprecipitated by anti-Flag (D) or anti-HA (E) magnetic beads were analyzed by immunoblotting. Note that HA-tagged PRRT2(1–268) was detected by anti-HA antibody in (D and E).

(F) Diagram for HA-tagged truncation of human PRRT2 (PRRT2(250–340)), in which the amino terminus of PRRT2 was deleted.

1150 **(G and H)** Co-immunoprecipitation assay for potential association between Nav1.2 and
1151 PRRT2(250–340). The proteins immunoprecipitated by anti-Flag (G) or anti-HA (H) were ana-
1152 lyzed by immunoblotting. Note that HA-tagged PRRT2(250–340) was detected by anti-HA an-
1153 tibody in (G and H).
1154 **(I and J)** Co-immunoprecipitation assay for potential association between Nav1.1 and
1155 PRRT2. The proteins captured by anti-Flag (I) or anti-HA (J) magnetic beads were analyzed
1156 by immunoblotting. In (A, B, D, E, G, H, I and J), blots shown are representative of at least
1157 three independent co-immunoprecipitation experiments with similar results. Red rectangles
1158 indicate the immunoblotting of bait and potential prey proteins in co-immunoprecipitation. IB,
1159 immunoblot. IP, immunoprecipitation. MW, molecular weight.
1160

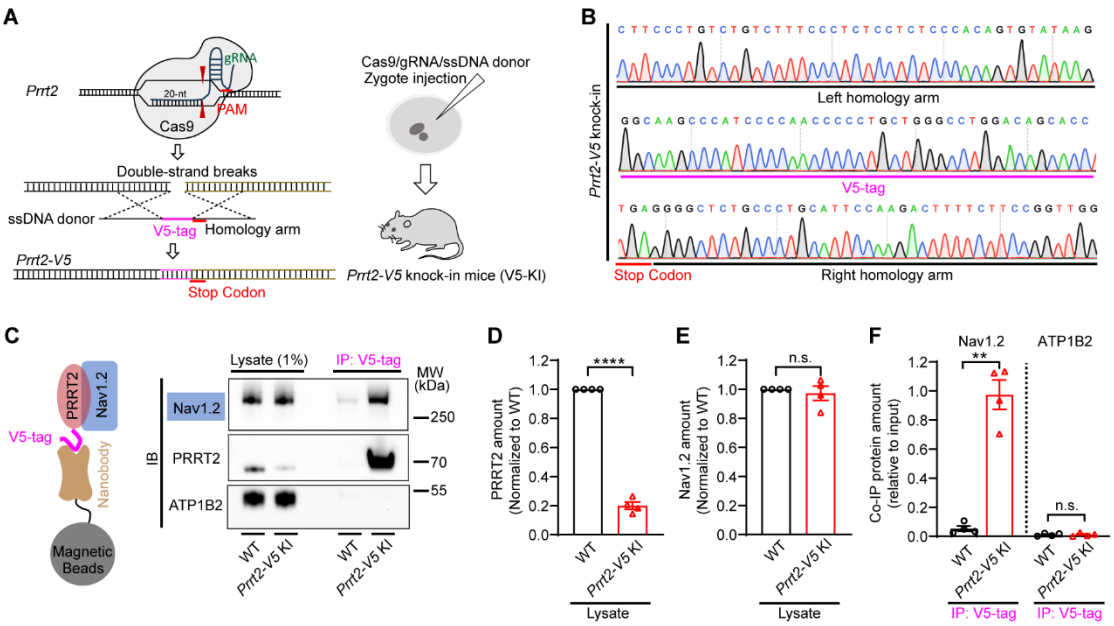

Figure 6 PRRT2 forms a molecular complex with Nav1.2 in the mouse brain

(A) Schematic showing the generation of *Prrt2-V5* knock-in (V5-KI) mice using Cas9 technology. V5-tag sequence was inserted precisely at the end of *Prrt2* gene. PAM, protospacer-adjacent motif (NGG). ssDNA, single-strand DNA.

(B) Sanger sequencing around sgRNA targeting site in *Prrt2-V5* knock-in mouse. The V5-tag, stop codon and homologous arms were denoted.

(C) Co-immunoprecipitation assay for potential interaction between Nav1.2 and PRRT2-V5 in the brain tissue. The proteins immunoprecipitated by anti-V5 nanobody were analyzed by immunoblotting. Blots shown are representative of four independent co-immunoprecipitation experiments. IB, immunoblot. IP, immunoprecipitation. MW, molecular weight. WT, wild-type. KI, knock-in.

(D-F) Quantification of the density of protein bands for PRRT2 (D) and Nav1.2 (E) in lysate, and for Nav1.2 and ATP1B2 in co-immunoprecipitation experiments (F) (n = 4 mice for each group). Data are presented as mean ± s.e.m. In (D-F), two-tailed, paired Student's t-test was used for determining statistical significance. $^{**}P < 0.01$, $^{****}P < 0.0001$, n.s., not significant.

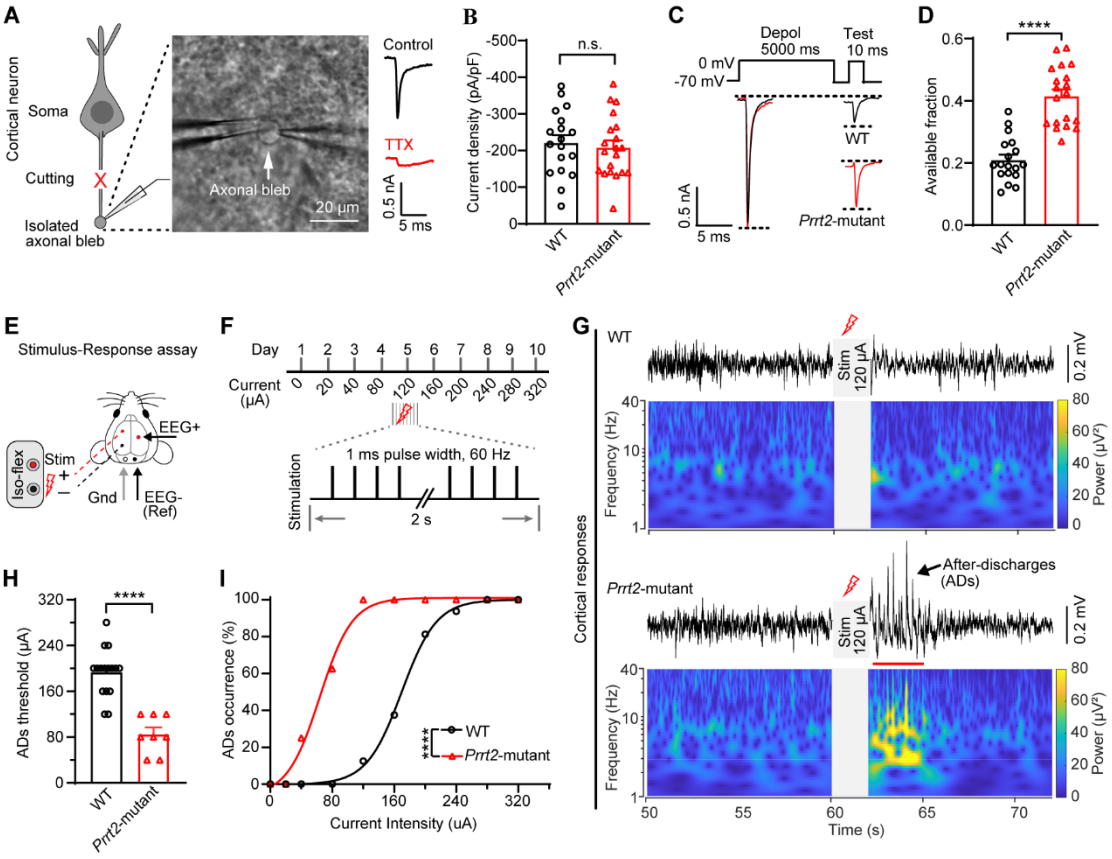

Figure 7 PRRT2 deficiency impairs the regulation of Nav channel slow inactivation and neuronal resilience in mice

(A) Schematic showing the isolated axonal bleb recording in cortical neuron (left) and the representative brightfield image for the axonal bleb in brain slice (middle). The arrow indicates an axonal bleb. Scale bar, 20 μm. The representative sodium current traces recorded in axonal blebs (right). Scale bar, 0.5 nA, 5 ms. TTX, tetrodotoxin.

(B) Sodium current density recorded in isolated axonal blebs from wild-type (WT) and *Prrt2*-mutant mice (WT: *n* = 18 blebs from 7 mice, *Prrt2*-mutant: *n* = 20 blebs from 8 mice). Sodium currents were measured with a brief depolarization to 0 mV preceded by a 200-ms hyperpolarizing prepulse to -110 mV.

(C) Protocol for assessing Nav channel slow-inactivation (upper) and the representative traces of the sodium currents evoked by conditioning depolarization pulse and test pulses (bottom). Scale bar, 0.5 nA, 5 ms.

(D) Fraction of available Nav channels after 5-s depolarization (WT: *n* = 18 blebs from 7 mice, *Prrt2*-mutant: *n* = 19 blebs from 8 mice).

(E) Schematic illustration of the cortical electrostimulation and EEG recording in mice. Ref,

1195 reference electrode. Gnd, ground electrode. Stim, Stimulation.

1196 **(F)** Illustration showing the experimental schedule and the stimulation parameters. Stimulation

1197 was delivered once daily with stepwise increases in current intensity.

1198 **(G)** Representative traces and power of EEG signals in wild-type and *Prrt2*-mutant mice be-

1199 fore and after 2-s cortical stimulation. After-discharges were indicated by the arrow and red

1200 line. Scale bar: 0.2 mV. Electrical stimulation (120 μA) was applied during 60–62 s period,

1201 where the stimulus-induced artifacts were removed prior to analysis.

1202 **(H)** Threshold of electrical stimulation to induce after-discharges in WT and *Prrt2*-mutant mice

1203 (WT: n = 16 mice, *Prrt2*-mutant: n = 8 mice).

1204 **(I)** Percentage of after-discharge occurrence in WT and *Prrt2*-mutant mice after electrical

1205 stimulation (WT: n = 16, *Prrt2*-mutant: n = 8). Data are presented as mean ± s.e.m. Two-

1206 tailed, unpaired Student's *t*-test was used in (B and D) and two-tailed, unpaired Mann-Whit-

1207 ney test was used in (H). In (I), the main effect of group was assessed using two-way ANO-

1208 VAs. ****P < 0.0001, n.s., not significant.

1209

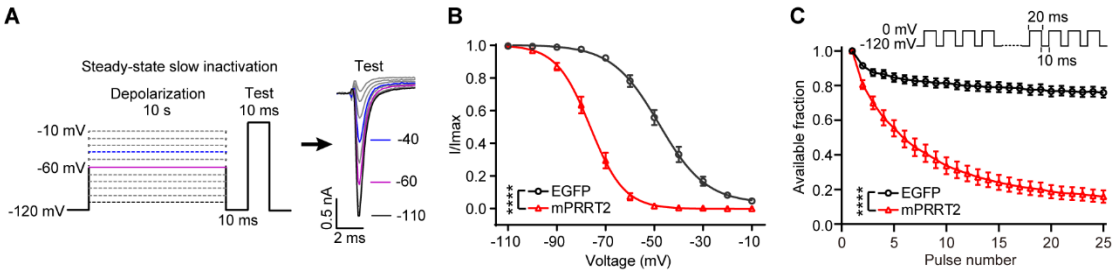

Figure 1-figure supplement 1. PRRT2 promotes steady-state slow inactivation and use-dependent inactivation

(A) Protocol of steady-state slow inactivation test (left) and representative traces of the sodium currents evoked by test pulses (right). The sodium currents gradually decreased as the voltage in conditioning steps increased. Scale bar, 0.5 nA, 2 ms.

(B) The effects of PRRT2 on voltage-dependent steady-state slow inactivation of Nav1.2 channels (EGFP: *n* = 11 cells, mPRRT2: *n* = 13 cells). mPRRT2, mouse PRRT2.

(C) PRRT2 modulates use-dependent inactivation of Nav1.2 channels during pulse trains (EGFP: *n* = 6 cells, mPRRT2: *n* = 6 cells). Data are presented as mean ± s.e.m. Two-way ANOVAs were used in (B and C) to determine the statistical significance of main effects of group. ****$P < 0.0001$.

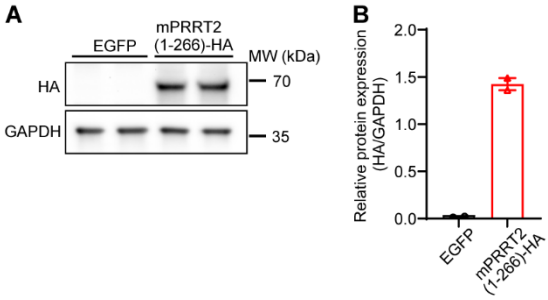

1224

1225 **Figure 2-figure supplement 1. Western blot verification of mPRRT2(1-266) expression**

1226 **(A)** Representative Immunoblot showing HA-tagged mPRRT2 (1-266) expression in Nav1.2-

1227 stably expressing HEK293T cells. GAPDH served as a loading control.

1228 **(B)** Quantification of mPRRT2(1-266)-HA expression normalized to GAPDH (*n* = 2 independ-

1229 ent experiments). Data are presented as mean ± s.e.m.

1230

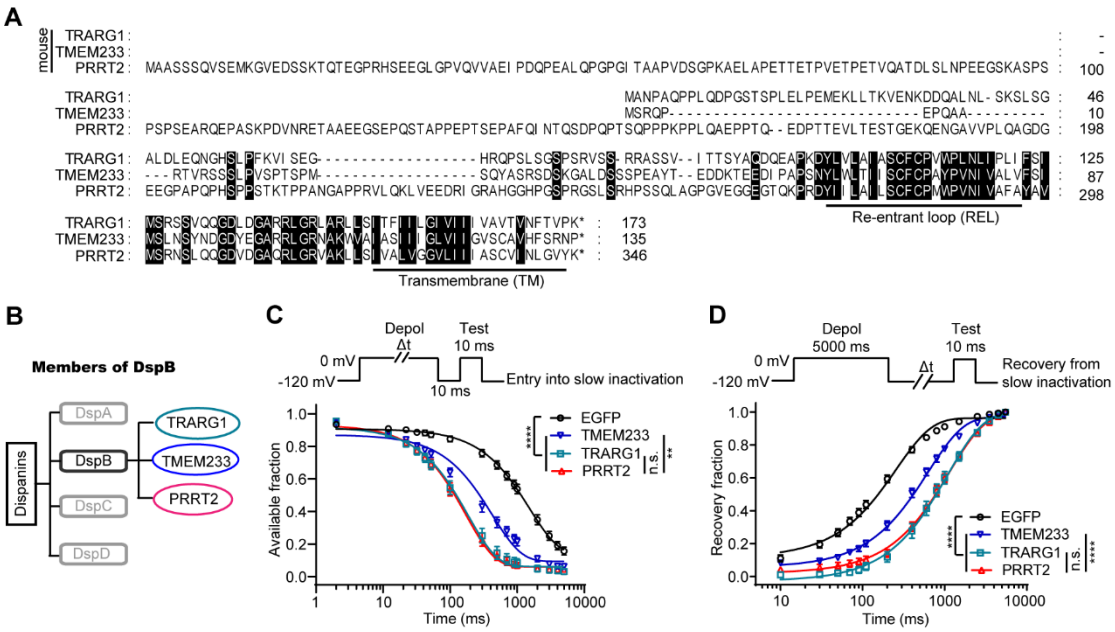

Figure 3-figure supplement 1. Paralogs of PRRT2 regulate Nav channel slow inactivation

(A) Sequence alignment of mouse TRARG1, TMEM233 and PRRT2 proteins. Conserved amino acids are highlighted and the transmembrane domains in carboxyl terminus of these proteins are underlined. REL, re-entrant loop. TM, transmembrane domain.

(B) Schematic showing the phylogenetic relationship between members of Dispanin subfamily B (DspB).

(C) The effects of members of DspB on the entry of Nav1.2 channels into slow inactivation (EGFP: *n* = 13 cells, TRARG1: *n* = 17 cells, TMEM233: *n* = 13 cells, PRRT2: *n* = 13 cells).

(D) The effects of members of DspB on the recovery of Nav1.2 channels from slow-inactivated states induced by 5-s depolarization (EGFP: *n* = 10 cells, TRARG1: *n* = 14 cells, TMEM233: *n* = 12 cells, PRRT2: *n* = 12 cells).

Data are presented as mean ± s.e.m. The main effect of group was assessed using two-way ANOVAs (C and D). $^{**}P < 0.01$, $^{****}P < 0.0001$, n.s., not significant.

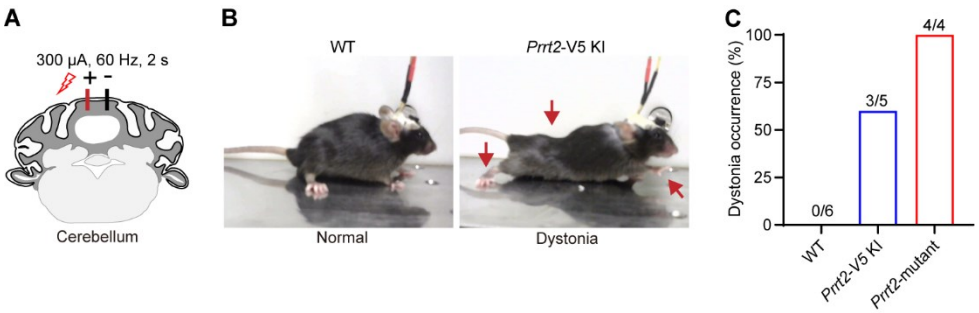

Figure 6-figure supplement 1. Dystonia behaviors in a subset of *Prrt2*-V5 knock-in mice

(A) Schematic illustration of electrical stimulation delivered to the localized area of the fourth/fifth cerebellar lobule in mice.

(B) Representative postures of wild-type (WT) and *Prrt2*-V5 knock-in (KI) mice following cerebellar stimulation. Arrows indicate the body parts affected during the dystonic episode.

(C) Incidence of dystonia behaviors induced by cerebellar electrical stimulation in WT, *Prrt2*-V5 KI, and *Prrt2*-mutant mice (WT: n = 6 mice, *Prrt2*-V5 KI: n = 5 mice, *Prrt2*-mutant: n = 4 mice). Data are presented as percentage of animals that exhibited dystonia behaviors within 5 minutes after stimulation.

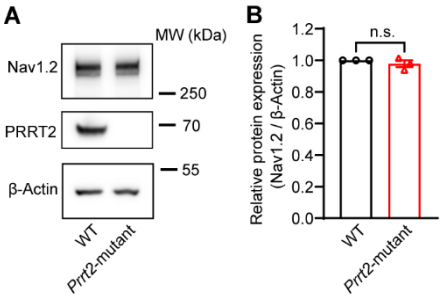

Figure 7-figure supplement 1. Protein levels of Nav1.2 are unchanged in brain tissue from *Prrt2*-mutant mice

(A and B) Immunoblots (A) and quantifications (B) of Nav1.2 proteins in brain tissue of wild-type (WT) and *Prrt2*-mutant mice (n = 3 mice). Data are presented as mean ± s.e.m. Two-tailed, paired Student's t-test was used in (B) to determine the statistical significance. n.s., not significant.

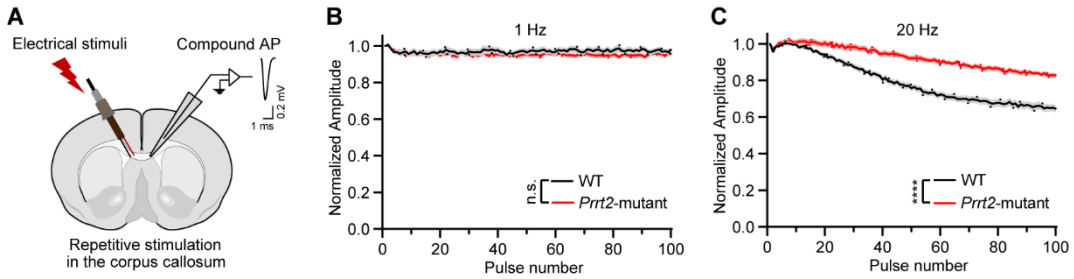

Figure 7-figure supplement 2. Activity-dependent adaptation is impaired in *Prrt2*-mutant mice

(A) Schematic illustration of corpus callosum stimulation and compound action potential (AP) recording in acute brain slices. Insert: representative trace of a compound AP recorded from the corpus callosum. Scale bar, 0.2 mV, 1 ms.

(B and C) Normalized peak amplitude of compound APs in corpus callosum during repetitive electrical stimulation (100 μA) at 1 Hz (B) and 20 Hz (C) in WT and *Prrt2*-mutant mice (WT: n = 22 slices from 5 mice, *Prrt2*-mutant: n = 20 slices from 4 mice). Data are presented as mean ± s.e.m. Two-way ANOVAs were used in (B) and (C) to determine the statistical significance of main effect of genotype. ****$P < 0.0001$. n.s., not significant.